AGU PUBLICATIONS

Reviews of Geophysics

REVIEW ARTICLE
10.1002/2017RG000557

Key Points:
- Most mechanical weathering at and near Earth's surface is likely driven by superimposed sources of low-magnitude subcritical stresses
- Weathering by subcritical cracking and concomitant regolith production and erosion are climate-dependent regardless of the stressing process
- Climate's influence on subcritical cracking varies with magnitude of the applied stress and with rock mechanical properties

Correspondence to:
M.-C. Eppes,
meppes@uncc.edu

Citation:
Eppes, M.-C., and R. Keanini (2017), Mechanical weathering and rock erosion by climate-dependent subcritical cracking, *Rev. Geophys.*, *55*, doi:10.1002/2017RG000557.

Received 7 FEB 2017
Accepted 3 MAY 2017
Accepted article online 7 MAY 2017

Mechanical weathering and rock erosion by climate-dependent subcritical cracking

Martha-Cary Eppes[1] **and Russell Keanini**[2]

[1]Department of Geography and Earth Sciences, University of North Carolina at Charlotte, Charlotte, North Carolina, USA, [2]Department of Mechanical Engineering and Engineering Science, University of North Carolina at Charlotte, Charlotte, North Carolina, USA

Abstract This work constructs a fracture mechanics framework for conceptualizing mechanical rock breakdown and consequent regolith production and erosion on the surface of Earth and other terrestrial bodies. Here our analysis of fracture mechanics literature explicitly establishes for the first time that all mechanical weathering in most rock types likely progresses by climate-dependent subcritical cracking under virtually all Earth surface and near-surface environmental conditions. We substantiate and quantify this finding through development of physically based subcritical cracking and rock erosion models founded in well-vetted fracture mechanics and mechanical weathering, theory, and observation. The models show that subcritical cracking can culminate in significant rock fracture and erosion under commonly experienced environmental stress magnitudes that are significantly lower than rock critical strength. Our calculations also indicate that climate strongly influences subcritical cracking—and thus rock weathering rates—irrespective of the source of the stress (e.g., freezing, thermal cycling, and unloading). The climate dependence of subcritical cracking rates is due to the chemophysical processes acting to break bonds at crack tips experiencing these low stresses. We find that for any stress or combination of stresses lower than a rock's critical strength, linear increases in humidity lead to exponential acceleration of subcritical cracking and associated rock erosion. Our modeling also shows that these rates are sensitive to numerous other environment, rock, and mineral properties that are currently not well characterized. We propose that confining pressure from overlying soil or rock may serve to suppress subcritical cracking in near-surface environments. These results are applicable to all weathering processes.

Plain Language Summary There is a long-standing question of how climate, particularly water, may influence the *physical* breakup of rock when it is exposed to the elements. It is typically assumed that the importance of water in rock cracking arises from the role that it plays in processes like freeze-thaw that require water to proceed. Here, we use classical mathematical models combined with a compendium of fracture mechanics theory and data from engineering research to show, for the first time, that water likely influences all types of rock cracking at Earth's surface whether it "requires" water or not. We also show that cracking proceeds even when only extremely low stresses are applied to the rock (akin to very small pulling forces). These stresses can be due to occurrences as simple and ubiquitous as daily heating and cooling by the sun.

1. Introduction

Physical rock breakdown (aka mechanical weathering; here comprising all in situ rock fracturing at and near Earth's surface) represents a critical rate-limiting factor for a broad range of geologic and geomorphic processes [e.g., *Shobe et al.*, 2017; *Collins and Stock*, 2016; *Lebedeva and Brantley*, 2017; *Heimsath et al.*, 1997; *Kirchner et al.*, 2006; *McAuliffe et al.*, 2006; *McFadden*, 2013]. There has been a limit, however, in our understanding of the dominant drivers of mechanical weathering on Earth and other terrestrial planets. In particular, moisture is widely cited as a substantial contributor to rock breakdown. Strong empirical relationships have been extensively documented between moisture and associated weathering, regolith production (defined here as the conversion of bedrock into mobile sediment), and/or erosion [e.g., *Burnett et al.*, 2008; *Griggs*, 1936; *Haas et al.*, 2015; *Hall*, 1986; *Larsen et al.*, 2014; *Matsukura and Takahashi*, 2000; *Owen et al.*, 2011; *Sass*, 2005]. Overall, however, the mechanisms by which water—in either liquid or vapor form—influence mechanical weathering have remained unclear [*Burke et al.*, 2007; *Hall and Hall*, 1996; *Halsey et al.*, 1998; *Mol and Viles*, 2012; *Sass*, 2005]. Therefore, it is most often tacitly accepted that the presence of water

accelerates mechanical weathering, while simultaneously assuming that some moisture-dependent, stress-causing processes like freezing dominate [e.g., *Elliott*, 2008; *Gerber and Scheidegger*, 1969; *Humphreys and Wilkinson*, 2007; *Moores et al.*, 2008; *Small et al.*, 1999; *Wells et al.*, 2005; *West et al.*, 2014].

In addition, the growing global database of rock denudation rates, including those describing bare rock [e.g., *Moses et al.*, 2014] and regolith production [e.g., *Vázquez et al.*, 2016; *West et al.*, 2013]—both closely tied to mechanical weathering—suggests that they are not universally predictable by traditional climate parameters like mean annual precipitation [e.g., *Heimsath et al.*, 2012; *Levenson et al.*, 2017; *Persico et al.*, 2011; *Portenga and Bierman*, 2011; *Ryb et al.*, 2014; *Von Blanckenburg*, 2005]. Thus, overall, there appears to be a clear need for understanding more precisely how climate influences mechanical rock breakdown processes. Here we build on existing rock mechanics and weathering literature to develop a fracture mechanics approach to this problem. In doing so, we illustrate and quantify a mechanistic link between climate and mechanical weathering.

The physical breakdown of rock necessarily stems from the propagation of fractures or cracks. The propensity for any given crack to propagate in a brittle-elastic solid like rock can be described through well-defined fracture mechanics laws that are generally categorized as either equilibrium or kinetic laws. Equilibrium laws predict that cracks will dynamically propagate once some "critical" stress (σ) is reached that exceeds the strength of the material. This strength is dictated by material properties such as tensile strength (σ_T) or fracture toughness (K_c aka critical stress intensity factor), which are themselves dependent on inherent material properties like Young's modulus or Poisson's ratio. With few exceptions [e.g., *Eppes et al.*, 2016; *Lamp et al.*, 2017; *Walder and Hallet*, 1985], environmentally driven weathering studies in particular have almost invariably applied an equilibrium law approach, asking: Does $\sigma_{process}$ exceed $\sigma_{critical}$? [e.g., *Al-Omari et al.*, 2014; *Bost and Pouya*, 2016; *Jiménez-González et al.*, 2008; *Ravina and Zaslavsky*, 1974; *Roering et al.*, 2010; *Wang and An*, 2016].

It is well accepted from the fracture mechanics literature, however, that cracks grow slowly and steadily — subcritically—at stresses much lower than critical stresses, even in rock [e.g., reviews in *Anderson*, 2005; *Atkinson*, 1984]. Long-term exposure (10^1–10^6 years) to such subcritical stress conditions is likely characteristic of all subaerial and near-surface rock environments.

Subcritical cracking is not predicted by equilibrium laws. Instead, it is described by kinetic laws, whereby cracking rates are dependent on factors including the stress magnitude as well as the geometry of the crack itself. Furthermore, and importantly, environmental conditions like moisture and temperature strongly temper the velocity of subcritical cracking [e.g., reviews in *Anderson*, 2005; *Meredith and Atkinson*, 1985; *Waza et al.*, 1980], *independent* of their influence on the stress loading (Figure 1). A few recent geomorphic studies have begun to explore subcritical cracking as it may apply to topography-related stresses [e.g., *Collins and Stock*, 2016; *Leith et al.*, 2014; *Molnar*, 2004; *Stock et al.*, 2012], thermal stresses [*Aldred et al.*, 2015; *Delbo et al.*, 2014; *Gischig et al.*, 2011b], or weathering of engineered stone cladding [*Chau and Shao*, 2006]; but to our knowledge, *the climate dependence of subcritical cracking itself* has not been closely examined and quantified in the context of Earth surface processes.

In this paper, we first analyze engineering and geophysics research to show that climate-dependent subcritical cracking is likely the primary mechanism by which all surface and near-surface rocks break down under natural conditions. We then combine foundational fracture mechanics laws and concepts from this literature to develop a relatively simple model that predicts fracture propagation rates for a range of generic stress magnitudes and climate conditions. We use the model, with existing rock-property data, to calculate erosion rates for granitic rocks exposed to a single source of stress, and a range of subaerial climate conditions. Our calculations are formulated to be applicable to any type of stress experienced by any rock at Earth's surface; however, we examine the specific, simple case of intergranular stresses arising from diurnal thermal cycling because these are minimum stresses that virtually all surface and near-surface rocks experience. As such, our model allows us to explore the sensitivity of weathering and erosion—caused by subcritical cracking—to stress magnitude and climate, as well as to inherent rock mechanical properties. In doing so, we begin to highlight the key elements of a process that is fundamental to most natural rock breakdown. These results have broad implications for understanding chemical weathering, sediment supply, regolith production, and erosion on Earth and other planets.

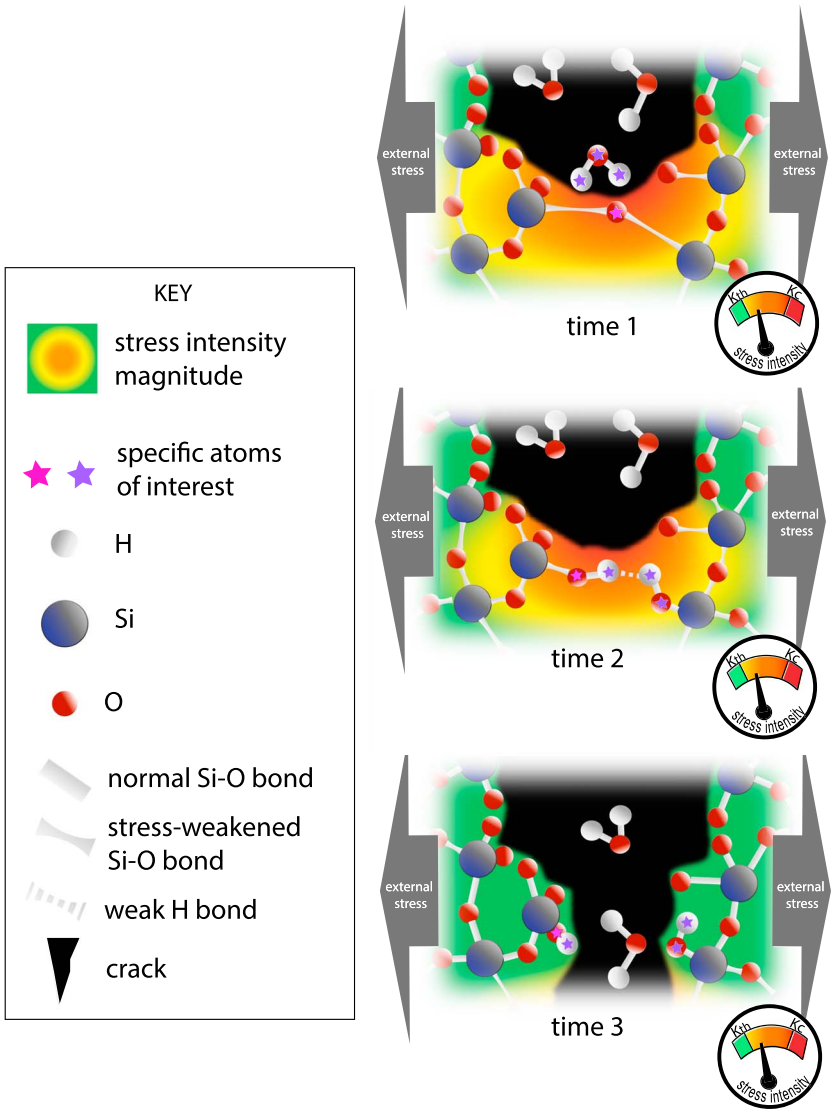

Figure 1. Conceptual schematic of climate-dependent subcritical cracking. The example shown is for stress corrosion in quartz (section 2). In all panels, external stresses loading magnitude is identical. The stress intensity factor (K) increases with proximity to the crack tip because flaws—like the crack depicted—concentrate stresses in a magnitude that is proportional to the length of the crack. (Changes in K driven by crack growth in Time 3 are not depicted.) Time 1: the molecular bonds bridging a crack tip are stretched due to external loading and are therefore weakened (here the molecules that include the highlighted atom). Time 2: because of the weakening, those "stretched" molecules become chemically reactive with water in the crack (here Si–O–Si is replaced by Si–OH–OH–Si). These reactions can occur with water in either vapor or liquid form, just as—for example—Fe oxidation. For subcritical cracking, however, the chemical reaction occurs solely at the crack tip, without disassociation of the water molecules or formation of reaction products, necessarily occurring. Time 3: the newly formed bonds are weaker than the previous bonds. Consequently, they are readily broken by the subcritical stresses that the rock is experiencing and the crack lengthens. As long as the experienced stress intensity (pointer on the stress meter) is higher than the threshold stress intensity (K_{th}) but lower than the fracture toughness of the rock (K_c), the process will repeat and subcritical cracking will proceed. Importantly, any external factor that might influence the chemical reaction (humidity, water availability, temperature, pore water chemistry, and rock composition) will—together with the applied external loading—serve to influence the rate at which the crack propagates.

2. Existing Literature Implicates Climate-Dependent Subcritical Cracking in Surface and Near-Surface Rock Weathering

2.1. Review of Terms and Concepts

2.1.1. Weathering and Erosion

Mechanical weathering commonly occurs at and near Earth's surface in excess of regional scale brittle failure (jointing) attributable to tectonic plate motions. Herein we define "near" as roughly $<$100 m, based on common observations that chemically and physically altered bedrock extends to these depths [e.g., *Bazilevskaya et al.*, 2013]. Observable cracking that comprises this weathering is ubiquitous in all rock and all

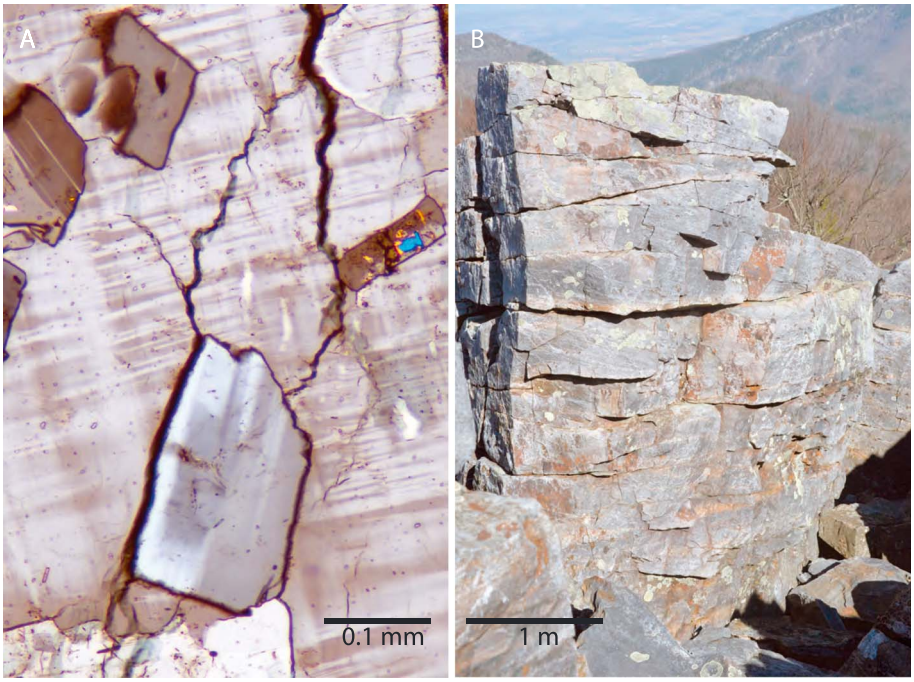

Figure 2. Photographs of typical cracks generated through weathering processes. (a) An oriented photomicrograph of cracks formed within 10 mm of the natural surface (up in the image) of a large, exposure of granite on an exfoliation dome in central North Carolina, United States. (b) Larger scale fractures formed along bedding planes in a natural outcrop of a quartz-rich meta-sandstone, Virginia, United States.

environments, including those of other planets [*Eppes et al*., 2015b], and it ranges in scale from micrometers to meters (Figure 2).

The sources of stress that lead to mechanical weathering can generally be divided into three broad—and likely interacting—categories: topographic, tectonic, and environmental. Here we define topographic stresses as those that arise from gravitational forces acting in concert with the weight of overlying rock or soil —or lack thereof for the case of unloading—at some depth [e.g., *Leith et al.*, 2014; *Molnar*, 2004]. Tectonic stresses arise due to ongoing plate motions in Earth's crust that can also interact with topography to enhance stress [*Martel*, 2006]. Finally, we define environmental stresses as those that comprise all climate- and environment-related stresses including freezing [e.g., *Draebing et al.*, 2017], salt precipitation [e.g., *Amit et al.*, 1993], mineral hydration [e.g., *Burnett et al.*, 2008], biologic activity [e.g., *Viles*, 2012], and thermal cycling [e.g., *Freire-Lista et al.*, 2016]. Both tectonic and topographic stresses might be considered static, but virtually all environmental stresses are cyclic at some periodicity (e.g., diurnal, seasonal, and annual).

For individual boulders, environmental stresses likely dominate. For bedrock, however, none of these sources of stress are likely mutually exclusive, and they have been shown to effectively interact to subcritically crack rock [*St. Clair et al.*, 2015; *Collins and Stock*, 2016; *Martel*, 2006]. Also, such superposition of stresses is expected by fracture mechanics theory (section 2.2.7). Herein, though, we focus on environmental stresses with the understanding that most concepts discussed also apply to both tectonic and topographic stresses, and that subcritical cracking in most bedrock is due to all three to some extent.

2.1.2. Fracture Mechanics

Whether critically or subcritically, all fractures propagate due to stresses that arise at crack tips where bonds must be permanently broken for a crack to grow. Stresses are typically divided into Mode I (tension), Mode II (in-plane shear), and Mode III (out of plane shear; tearing). Tensile stresses are the most important and dominant in driving fracture propagation and therefore are the primary mode of stress considered herein.

Because fractures or other flaws in brittle elastic solids serve to amplify stresses above external loading levels, the magnitude of stress concentrated at any given crack tip is described by the *stress intensity factor*, *K*. Stress intensity is calculated differently for different stress loading and/or crack geometries, but the term is most

generically defined for Mode I fracture as $K_I \approx \sigma\sqrt{\pi a}$, where σ is the stress induced by the external load and a is one half of the crack length. As such, the magnitude of the stress intensity factor at a crack tip (hereafter referred to as stress intensity) is a product of both external loading as well as the size of the flaw itself. There is also thought to be a stress intensity threshold, K_{th}, below which no fracture growth occurs at all (section 2.2.8). Below K_c, but above K_{th}, fractures grow subcritically.

Examining subcritical cracking in the context of stress intensity illustrates that as a crack grows, the amount of external loading required for it to propagate decreases. This concept is an important one for mechanical weathering because it means that over geologic time, very low stresses can increase crack lengths to the point where some—seemingly random—small stress may serve to exceed the fracture toughness, K_c of the material, and the rock will break catostrophically.

There are many well recognized and hypothesized chemical and physical processes acting at crack tips to subcritically propagate fractures once K_{th} is exceeded. Many are strongly debated and not well-understood [*Anderson*, 2005]. All, however, involve stressed microcracks that propagate because of chemical reactions between pore water and the cracking material (e.g., reviews in *Atkinson* [1984] and *Brantut et al.* [2013]). These chemical reactions are uniquely efficacious at crack tips where crystal lattice bonds are stretched and thus weakened, allowing the chemical reaction to occur there; subsequently, the crack lengthens rather than widens (Figure 1). Environmental factors like temperature and moisture availability influence these reaction rates and therefore influence cracking rates. Such processes have only rarely been referenced in weathering or geomorphology literature [*Hooke*, 1991; *Ishikawa et al.*, 2004; *Molnar*, 2004; *Tharp*, 1987; *Walder and Hallet*, 1985; *Williams and Robinson*, 1991].

Terms including "environmentally assisted cracking," "stress corrosion," "time-dependent crack growth," "progressive failure," "microcracking" or "static fatigue" are commonly synonymously employed to describe combined subcritical cracking processes. In particular, the term stress corrosion is frequently employed to describe a suite of possible chemophysical processes acting at crack tips in concert with stress loading [*Parkins*, 2005]. In some cases, though, the term is limited to a more strict definition, and one of the other terms listed above is employed instead to cover all such processes [e.g., *Anderson*, 2005]. Nevertheless, stress corrosion—in its generic form—is extensively cited as the dominant contributing mechanism of subcritical crack growth in stressed crustal rock (e.g., reviews in *Anderson and Grew* [1977], *Atkinson* [1984, 1987], *Brantut et al.* [2013], and *Meredith* [1990]). It should be noted, however, that extremely few subcritical cracking studies identify the specific process acting at crack tips in studied rock [*Brantut et al.*, 2014a]. Thus, herein all such environmentally dependent processes that serve to propagate fractures under subcritical loading, both cyclic and static, are lumped under the term subcritical cracking.

2.2. The Case for Subcritical Cracking in Subaerial and Near-Surface Rock

2.2.1. Overview

At a minimum, subcritical cracking by any environmentally assisted process, regardless of the chemical reaction or material being fractured, requires (1) a preexisting heterogeneity like a microfracture, (2) moisture in the form of liquid water *or* humidity, and (3) stress loading [*Brantut et al.*, 2013], all of which likely universally exist in surface or near-surface rock clasts or bedrock. Rates of subcritical cracking in rock are characterized through both theoretical evaluations, as well as laboratory experimentation. In the latter, rocks are subjected to varying environmental conditions and stresses, and subcritical cracking is then measured either directly, through visual evaluation or acoustic emission monitoring, or indirectly through measurement of changes in acoustic velocities.

A large body of experimental studies document that subcritical cracking velocity is dependent on a number of environmental factors including the magnitude of applied stress [e.g., *Atkinson and Meredith*, 1987], rock composition [e.g., *Nara et al.*, 2011; *Potyondy*, 2007], pore humidity [e.g., *Nara et al.*, 2010], pore water chemistry [e.g., *Jeong et al.*, 2007], and temperature [e.g., *Heap et al.*, 2009a]. In the remainder of section 2, we highlight data that support these conclusions. Unless otherwise indicated, all literature cited in the remainder of this section is for work conducted on rock.

2.2.2. Susceptible Rock Types

All major rock types are susceptible to subcritical cracking [*Atkinson*, 1987]. The majority of research in rocks has been in the context of granite, most commonly Westerly granite [e.g., *Atkinson*, 1984; *Kranz*, 1979; *Lockner*, 1993]. Studies documenting subcritical cracking in other rock types are less common but include

quartzite and sandstone [*Atkinson*, 1984; *Brantut et al.*, 2014b; *Hadizadeh and Law*, 1991; *Heap et al.*, 2009b], gabbro [*Meredith and Atkinson*, 1985], basalt [*Heap et al.*, 2011], andesite [*Nara et al.*, 2010, 2013], iron ore [*Grgic and Amitrano*, 2009], and carbonate rocks [*Brantut et al.*, 2014a; *Nicolas et al.*, 2014; *Røyne et al.*, 2011]. The presence of clay can accelerate subcritical cracking [*Nara et al.*, 2011], an important finding to consider as rocks become weathered.

In general, all subcritical cracking can proceed without preexisting cracks, senso stricto. All rocks are heterogeneous at small spatial scales and contain inherent flaws like pores, grain boundaries, vesicles, or mineral cleavage that can amplify stresses [e.g., *Heap et al.*, 2014] and lead to subcritical cracking [e.g., *Raja and Shoji*, 2011]. Thus, in the context of rock, there is no need to discuss crack initiation as strictly defined in fracture mechanics literature pertaining to, for example, steel. The size, density, and shape of existing flaws in rock—as well as their orientation with respect to stress—can, however, strongly influence subcritical cracking rates [*Griffiths et al.*, 2017]. This conclusion represents another key consideration in the context of long-term weathering because such characteristics change through time.

2.2.3. The Chemophysical Processes

The exact chemical reaction that occurs during subcritical cracking will vary with material, or in the case of rocks, the minerals present in the rock. There are numerous documented and proposed chemical reactions, but the most well established is for a type of stress corrosion in silicate minerals, particularly quartz [e.g., *Atkinson*, 1979; *Dove*, 1995; *Michalske and Freiman*, 1982].

In quartz, strained Si–O bonds at crack tips (Figure 1, Time 1) can readily react with pore water due to the resulting decrease in overlap of atomic orbitals. There, weakly bonded Si–OH–OH–Si molecules replace strongly bonded Si–O–Si molecules as water is incorporated into the quartz's chemical structure through electron and proton transfers (Figure 1, Time 2). Then, these new weaker bonds are readily broken by the existing stress, and the crack extends (Figure 1, Time 3). The efficacy of this reaction is less explored in—but thought to be viable for—other commonly occurring silicate minerals such as micas and feldspars. Additional reactions for biotite, feldspars, and calcite have also been proposed [e.g., *Barnett and Kerrich*, 1980]. Other cited and less well-characterized chemical processes that facilitate subcritical cracking in rock include diffusion mass transport, ion exchange, and dissolution [e.g., *Atkinson*, 1987; *Brantut et al.*, 2014b].

Cyclic fatigue, whereby bonds are weakened and then broken due to cyclic loading, is another process that is a well studied but somewhat debated mechanism of subcritical cracking for the case of rock [e.g., *Attewell and Farmer*, 1973]. While it is relatively commonly considered in weathering studies [e.g., *Hall and Thorn*, 2014; *Halsey et al.*, 1998], cyclic fatigue has less commonly been *quantified* in terms of weathering-sourced stress and crack propagation [e.g., *Brain et al.*, 2014; *Delbo et al.*, 2014; *Jia et al.*, 2015; *Molaro et al.*, 2017]. The fatigue process is complicated, however, by numerous factors such as friction on fracture surfaces that are not typically considered by weathering scientists [e.g., *Scholz and Kranz*, 1974; *Scholz and Koczynski*, 1979].

While cyclic fatigue-driven subcritical cracking can theoretically proceed under zero humidity with no chemical reaction process necessary, it is widely understood that stress corrosion—or other environmentally driven cracking as described above—proceeds under cyclic loading [*Jones*, 1992]. Thus, cyclic fatigue cannot be isolated—except perhaps in a vacuum under 0% humidity—from these other environmentally driven subcritical cracking processes. Instead, cyclic fatigue serves to both simultaneously and independently propagate microfractures experiencing cyclic loading conditions [e.g., *Costin and Holcomb*, 1981]. We quantitatively explore the relationship between cyclic- and static-driven subcritical cracking in Appendix A and demonstrate that they are equivalent.

2.2.4. Moisture and Temperature Dependence

In a broad range of rock types, subcritical cracking rates are experimentally shown to increase with increasing atmospheric relative humidity, with the presence of liquid water and with increasing temperatures—within the range of those experienced on Earth's surface [*Heap et al.*, 2009a; *Holder et al.*, 2001; *Kranz et al.*, 1982; *Meredith and Atkinson*, 1985; *Nara et al.*, 2010, 2013, 2011]. Although rock type and water chemistry influence these relationships, most experimental data reveal order of magnitude increases in subcritical cracking velocity with linear increases in factors like relative humidity or temperature in virtually all rock types studied. For example, rates of cracking in dolerite increased by 2–3 orders of magnitude—under the same stress intensity—when subjected to wet conditions at 20°C versus 75°C [*Meredith and Atkinson*, 1983]. Few experimental data exist for temperatures below freezing.

Liquid water is not necessary for subcritical cracking to proceed. Experiments in rock are commonly conducted under environments ranging from low humidity (30%) up to fully saturated conditions [*Brantut et al.*, 2013], and measurable subcritical cracking occurs throughout the full range of relative humidity, without the presence of liquid water [*Jeong et al.*, 2007; *Nara et al.*, 2010, 2013]. In virtually all of the experimental data demonstrating the moisture dependence of subcritical cracking, the slope of the velocity curve itself remains constant, possibly suggesting that the subcritical cracking mechanism itself remains constant [*Røyne et al.*, 2011].

Relative humidity at Earth's surface averages between 70% and 80% for most land areas besides deserts and high elevations, which average 30–60% [*Dai*, 2006]. Information regarding the internal moisture levels of rock or bedrock under soil are currently relatively limited [*McAllister et al.*, 2017, 2016; *Rode et al.*, 2016; *Sass*, 2005; *Stück et al.*, 2013]. Accurate measurements of how humidity translates to long-term rock interior moisture will be necessary, however, for accurate predictions of subcritical cracking rates in weathering environments. Measured degrees of saturation in exposed rock range from 10 to 100% in the upper few meters and average 30–50% [review in *Sass*, 2005], but even in relatively dry Antarctic climate, granite surfaces have been measured to be wet 40% of the time during summer months [*Elliott*, 2004]. Surface topography and shading can result in variable rock moisture conditions at relatively small space scales [*Schnepfleitner et al.*, 2015].

Few studies have measured long-term daily rock surface temperatures. Short-term data from different environments suggest that rock surface temperature minimums are on the scale of that of air, whereas maximums are commonly ~10°C higher than ambient air temperature [*Eppes et al.*, 2016; *Hall and André*, 2001; *McKay et al.*, 2009; *Sumner et al.*, 2004, 2007]. Temperature measurements in rock interiors are much less common; they are tempered by rock thermal diffusivity [*Anderson*, 1998; *Smith et al.*, 2011]. The global annual averages of daily air *temperature range* spans from ~5° to ~25°C, with the majority of the Earth's land surface falling between 10° and 20°C [*Chan et al.*, 2016; *Harris et al.*, 2014]. Annual averages of daily rock surface temperature range data are also rare but are reported between about 30°C for semiarid temperate climates and about 25°C for humid temperate climates [*Eppes et al.*, 2016; *Sumner et al.*, 2004].

2.2.5. Water Chemistry Dependence

Pore water chemistry influences subcritical cracking rates, but there is somewhat limited knowledge of the precise nature of these effects for rock. Nevertheless, simple water vapor—over organic vapor like methanol for example—has been cited and demonstrated as one of the most effective subcritical cracking agents [*Jeong et al.*, 2007]. Subcritical crack growth in rock also appears to be pH dependent. In quartz this is especially the case at low stress intensity values, where crack velocities are significantly higher in basic water [*Atkinson and Meredith*, 1981]. However, as with all geochemical reactions, the effect of pH is dependent on the exact constituents of the solution and the mineral involved. For example, subcritical cracking velocities for calcite generally increase with increasing pH; but in the presence of some bases (e.g., NaOH), they do not [*Dunning et al.*, 1994].

The typical pH of meteoric waters under a broad range of environmental conditions is between about 4.1 and 5.5. Global estimates of soil water pH range between ~4.5 and 8.5 [*Batjes*, 1995]. Measurements of the pore water chemistry of surface rocks are relatively rare. However, those values are likely more akin to that of soil rather than rainwater and will likewise vary with vegetation and temperature. For example, median soil pH for shallow (0–30 cm) soils weathering directly from bedrock have been measured between 5.6 for siliceous rocks like granite and 7.6 for carbonates and 7.7 for basalts [*Batjes*, 1995]. Measures of pH of pools forming in granite quarries in cool temperate environments seasonally and diurnally ranged between 6.2 and 6.8 depending on temperature [*Reed and Klugh*, 1924]. Experiments flushing distilled water through ground quartz particles revealed similar values [*Atkinson and Meredith*, 1981].

2.2.6. Effects of Confining Pressures

Rates of subcritical cracking generally decrease or are halted with increasing confining pressures [*Brantut et al.*, 2014a; *Christensen and Wang*, 1985; *Heap et al.*, 2009b, 2011; *Zoback and Byerlee*, 1975]. Nevertheless, the majority of experiments have in fact been conducted under atmospheric pressure [*Brantut et al.*, 2013] where crack velocities are presumably the highest. For bedrock, topographic stresses [*Molnar*, 2004] and effects or tectonic stresses [*Martel*, 2006, 2011] likely serve to offset confining pressures to some degree and are potentially additive to other environmentally related loading [*Clair et al.*, 2015; *Gischig et al.*, 2011a; *Stock et al.*, 2012].

In a relatively simple view lithostatic, or confining pressure, P, increases linearly with subsurface depth, z, according to $P(z) = P_o + \rho g z$. Here ρ and g are bulk rock density—which itself will change with depth—and gravitational acceleration, respectively, and P_o is the pressure at some datum, typically the rock surface [e.g., *Passchier and Trouw*, 2005]. It appears, however, that very little, if any, subcritical crack growth data explicitly address the influence of relatively small sub-MPa confining pressures characterizing weathering environments, including those extant under soil cover. Depth to bedrock can vary over small spatial scales and might range from 10^{-1} to 10^{0} m in tectonically active settings where erosion is relatively rapid but may range from 10^{-1} to 10^{2} in slowly eroding landscapes [*Bazilevskaya et al.*, 2013]. We consider these effects in more detail in Appendix B.

2.2.7. Stress-Dependence and Weathering-Related Stresses

Regardless of rock type, subcritical cracking rates are consistently shown in experimental and theoretical studies to increase with increasing magnitude of applied tensile stress (e.g., review in *Amitrano and Helmstetter* [2006]). This relationship is due not only to higher mechanical tensile stresses induced by loading but also to enhanced efficacy of subcritical cracking-related chemical reactions under higher stresses; the latter, in turn, arises because of weaker bond strengths that manifest at crack tips under loading. In some cases, however, only limited cracking acceleration is observed under a narrow zone of stress magnitudes intermediate between K_c and K_{th} (referred to as Region II subcritical cracking) when moisture availability is low—due to permeability, for example [e.g., *Nara et al.*, 2017]. This effect is due to the inability of moisture to transmit to crack tips at these cracking velocities; as stresses approach K_c the process becomes more mechanical and influenced by the rock strength [e.g., *Atkinson*, 1987].

Numerical modeling and laboratory tests confirm that rates of subcritical cracking under *static* loading are dependent on mean stress *magnitude*, whereas those rates under *cyclic* loading are sensitive to the *amplitude* of the stress cycles [*Costin and Holcomb*, 1981; *Heap and Faulkner*, 2008; *Scholz and Koczynski*, 1979]. With respect to cyclic loading, the number of cycles to failure also depends on the loading *rate*. It is thought that at high stressing rates, there is insufficient time for subcritical cracking-related chemical reactions to proceed before a cyclic fatigue limit is reached by the material [*Costin and Holcomb*, 1981; *Hadizadeh and Law*, 1991]. In contrast, at relatively low stressing rates, subcritical cracking has sufficient time to produce further rock breakdown, resulting in an overall lower number of cycles necessary to trigger catastrophic failure [*Costin and Holcomb*, 1981].

In addition, the overall magnitude of external stresses required for subcritical cracking is lower when adjacent microfractures interact to produce a higher stress intensity than that of a solitary crack [e.g., *Costin*, 1985]. This phenomenon is due to the fundamental influence that crack proximity has on stress intensity overall [*Anderson*, 2005]. In such cases, crack growth is fastest in regions and/or directions of highest crack density or directions parallel to a preexisting microcrack fabric [e.g., *Kudo et al.*, 1992; *Nara and Kaneko*, 2006; *Zhao*, 1998]. As such zones of high microfracture or flaw density—for example, along bedding planes—will experience faster subcritical cracking, leading eventually to more prominent macrocracks, as is commonly observed in the field (e.g., Figure 2b).

Finally, overall stress intensity values for Mode I (tensile) subcritical crack opening are additive under the simultaneous action of differing Mode I loading mechanisms [*Anderson*, 2005]. In other words, the magnitude of the stress intensity for any given crack, at any given time, is calculated by adding the magnitude of all tensile stresses that the crack is experiencing. Therefore, in weathering environments, even very low-magnitude tensile loading mechanisms presumably act in concert to allow exceedance of the threshold stress, K_{th}, necessary for subcritical cracking to occur (see below). Acoustic emission data from instrumented boulders [*Eppes et al.*, 2016], as well as instrumentation and theoretical considerations of rock walls [*Collins and Stock*, 2016], support this picture, in that cracking is observed to preferentially occur under several—simultaneously acting—low-magnitude stresses.

2.2.8. Threshold Stress Intensity for Subcritical Cracking

There is no consensus on the magnitude of the lower stress intensity limit, K_{th}, below which subcritical cracking does not occur [e.g., *Atkinson*, 1987]. Some existing observational and modeling data suggest that stresses as low as 100 kPa can lead to fracture propagation and failure over time [*Gischig et al.*, 2011b]. It is most commonly held, however, in virtually all fracture mechanics applications, not just rock, that K_{th} is on the order of 10–20% of the fracture toughness, K_c of the material [e.g., *Anderson*, 2005; *Atkinson*, 1984]. For

example, the K_{th}/K_c ratio needed for splitting micas along cleavage planes in a wet environment has been measured at 0.1 [*Lawn*, 1993] and that of quartz at 0.15 [*Parks*, 1984].

It is important to note, however, that the experiments that produce K_{th} data can only constrain its upper limit, that is, the stress above which the material will unambiguously subcritically crack. It is not known the extent to which such experiments are translatable to extremely long timescales relevant to weathering processes, where stresses well below 0.1 K_c could still result in extremely slow cracking not readily measurable in a laboratory setting [*Heap and Faulkner*, 2008; *Heap et al.*, 2009b]. Further, the magnitude of K_{th} itself is strongly dependent on environmental and material properties [e.g., *Eberhardt et al.*, 1998], adding more ambiguity to the 0.1–0.2 K_c estimate for K_{th}. In our modeling below, we build an argument that generally supports K_{th} values of 0.2 K_c for granite; in reality, however, this parameter is one for which there is an overall lack of data in the context of weathering and erosion over geologic timescales.

Calculations of environmental stresses experienced in outcrops [*Holzhausen*, 1989; *Jiménez-González et al.*, 2008; *Tharp*, 1987; *Walder and Hallet*, 1985; *Wang and An*, 2016] and individual boulders [*Eppes et al.*, 2016; *Molaro et al.*, 2017; *Shi*, 2011; *Tanigawa and Takeuti*, 1983] are relatively rare. In these studies, maximum potential stresses calculated are typically on the order of kPa to a few MPa. Although stress magnitudes of these orders are generally lower than tensile strength values for most rock types, they are almost always within the range of K_{th} ~ –0.1 K_c to 0.2 K_c for the rock types considered. Thus, it would appear that most weathering-related stresses are not critical but are sufficient for subcritical cracking, even with conservative values of K_{th}. Lightning strikes may be one of the few exceptions [*Knight and Grab*, 2014].

3. Modeling Climate-Dependent Subcritical Cracking and Rock Erosion: Overview

In the remainder of the paper, we develop and validate simple, theoretical models of climate-dependent subcritical cracking and associated rock erosion for generic, granitic rocks exposed at Earth's surface. We employ realistic rock, environment, and stress-loading parameters that can be interchanged with those of other rock types or climates.

Modeling any subcritical cracking in rock requires that we first model a stress. Here we focus on intergranular stresses produced by diurnal thermal cycling, a ubiquitous, physically simple and well-understood process. All surface and near-surface rocks on Earth, as well as other planetary bodies, experience thermal cycling and therefore likely undergo some degree of thermally induced diminution [e.g., *Molaro et al.*, 2017; *Delbo et al.*, 2014; *Eppes et al.*, 2015b; *Aldred et al.*, 2015]. Thus, these universally occurring stresses represent a lower limit on all environmental stresses, regardless of climate, rock type, rock, or outcrop shape or size, and therefore make a good starting point for thinking of subcritical cracking in near-surface environments.

In the modeling, we focus on the following:

1. Modeling stresses as purely cyclic, we use Paris's law [*Paris et al.*, 1961] to describe the relationship between crack growth rate and stress

$$\frac{da}{dN} = C(\Delta K_I)^m \tag{1}$$

   where $a = a(N)$ is the crack length following the N^{th} load cycle, C and m are material- and climate-dependent constants, and ΔK_I is the amplitude of the cyclically varying Mode I stress intensity factor, K_I.
2. The effect of climate on crack growth, as modeled by equation (1), enters through the environment dependence of both the Paris law exponent, m, and to a lesser extent, the Paris law coefficient, C (summarized in textbooks such as *Anderson* [2005]). Unfortunately, for rock experiencing cyclic loading, virtually no data currently exist on either of these parameters nor on the subcritical cracking threshold, K_{th}. Thus, a significant original contribution of the current work is that we develop and validate estimates for these parameters that are suitable to their application in a weathering environment (section 5). Herein, we only quantify the relationship between moisture and these parameters, ignoring that other environmental factors such as temperature influence them and thus subcritical cracking rates.

Table 1. Rock Parameters Used in All Calculations Unless Otherwise Noted

Parameter	Symbol	Reference Magnitude; Range of Values	Reference Notes
Granite thermal diffusivity	κ	$1.5(10^{-6})$ m^{2}s^{-1}	*Holzhausen* [1989]
Granite (bulk) thermal expansion coefficient	α	$8(10^{-6})$°C^{-1}	*Holzhausen* [1989]
[a]Thermal expansion coefficient, quartz	α_1	Max: $5.667(10^{-5})$°C^{-1}Min: $4.5(10^{-5})$°C^{-1}	*Robertson* [1988], *Fei* [1995], and *Skinner* [1966]
[a]Thermal expansion coefficient, feldspar	α_2	Max: $1.75\ (10^{-5})$C°$^{-1}$Min: $0.61(10^{-5})$°C^{-1}	*Robertson* [1988], *Fei* [1995], and *Skinner* [1966]
Characteristic thermal expansion difference	$\Delta\alpha = \alpha_1 - \alpha_2$	2.75 to 5.06 (10^{-5})°C^{-1}	Calculated
Rock Poisson's ratio	ν	0.22	*Gercek* [2007]. IIntermediate value from compiled data in Figure 4
Diurnal half-cycle	Ω	12 h	Specified
Characteristic thermal penetration depth	$\delta_T = \sqrt{\kappa\Omega}$	0.25 m	Calculated
Granite (bulk) Young's modulus	E	50, 600 MPa	*Holzhausen* [1989]
Characteristic grain size (Westerly granite)	d_g	$0.7(10^{-3})$ m	*Chen* [2008]
Granite fracture toughness	K_c	1.7 MPa m$^{1/2}$	*Atkinson* [1987]. Average of compiled values (n = 57) in Table 11.6
Rock tensile strength (Barre granite)	σ_T	10 MPa	*Dai and Xia* [2010]
Subcritical crack growth index = Paris law exponent	$n = m$	Varying with $\langle RH\rangle$ [b]ex: for $\langle RH\rangle$ =10%, n = 77.6; for $\langle RH\rangle = 80\%, n = 58$	*Nara et al.* [2013]. Appendix A
Paris law coefficient	$C{\sim}d_g K_c^{-m}$	$C{\sim}0.7(10^{-3})$ m$\times(2.16$ MPa m$^{1/2})^n$; exponent $n = m$	Estimated Appendix D

[a]These are the maximum and minimum bulk values for these minerals as derived from all measured values found in the literature examined in this study ($n \sim 10$ for both). We do not consider the values for individual crystallographic axes of these minerals, which can vary greatly [*Meredith et al.*, 2001].
[b]Estimates based on a linear fit for $m : m(\langle RH\rangle) = m_0 - m_1 \times \langle RH\rangle$, where $m_0 = 80.4$ and $m_1 = 0.28$, as measured in Oshima granite by *Nara et al.* [2013].

3. The effect of temperature on subcritical cracking in our models enters only through the temperature dependence of the particular stress we characterize, intergranular stresses induced by diurnal thermal cycling, which we model using an existing [*Holzhausen*, 1989] analytical solution (Appendix C). The magnitude of these stresses is controlled not only by diurnal temperature range (section C1) but also by the rock's Poisson's ratio and differences in coefficients of thermal expansion of the rock's primary constituent minerals (section C2).
4. We incorporate thermal and physical parameter characteristics of granite into our models (Table 1) because it is a common rock type for which physical property data are generally available.
5. Once validated, we first employ the proposed subcritical cracking model to examine the influence of relative humidity alone on cracking rates under different stress magnitudes (section 7). We do so by treating the rock's experienced stress as a ratio to its fracture toughness. As such, these first results are applicable for most any source of cyclic stress.
6. We then combine the subcritical cracking model with the thermal stress model to calculate rates of weathering/erosion of subaerial granitic rock under different climate conditions (section 8). We idealize weathering/erosion as spalling/granular disaggregation, whereby once a representative, in-growing crack reaches the characteristic critical crack length, a_c, the small outer layer of rock grains of thickness a_c, spalls off. As such, our modeled erosion might be considered equivalent to the style of steady, surface-down rock erosion that is commonly assumed in studies of ^{10}Be-derived regolith production and rock erosion rates [e.g., *Heimsath et al.*, 1997].

The rock erosion model obtained—which neglects all other stress-loading and erosion processes—thus allows prediction of a range of "minimum" erosion rates. That range is obtained as a function of known ranges in various rock parameters and of the following climate parameters: (i) mean annual relative humidity and (ii) in the case of the thermal stresses that we explore here, the mean annual diurnal temperature variation.

4. Climate-Dependent Subcritical Cracking Model

4.1. Assumptions and Simplifications

We argue that simplified crack propagation modeling can provide insight into how climate-dependent subcritical cracking may act as a weathering process. We view our approach as a physically motivated alternative to using, for example, reaction rate theory for determining crack velocities [e.g., ala *Røyne et al.*, 2011], or multiscale, finite element, thermoelastic, and/or fracture modeling [e.g., *Delbo et al.*, 2014; *Molaro and Byrne*, 2015], both of which require numerous rock and environmental parameters that currently do not exist.

Thus, we believe that the proposed modeling approach—emphasizing physically based scaling arguments that lead to testable observations and conclusions—and focused on grain-scale cracking processes that are quantitatively well characterized, allows identification of key parameters that influence weathering-induced subcritical cracking.

Assumptions and simplifications in the model include the following:

1. We limit attention to grain-scale subcritical cracking on subaerially exposed rock surfaces that—on the scale of grain-size cracks—are nominally flat.
2. Thus, we focus solely on formation of intergranular surface cracks having initial lengths, a_o, on the order of the characteristic grain size, d_g. This assumption is consistent with the observation that microfracture lengths in unweathered rock are typically on the order of the constituent grain size [*Nasseri et al.*, 2005].
3. Further, we assume that the characteristic *critical* crack length, a_c, is also on the order of the characteristic grain size, again a reasonable assumption given the abundant field and laboratory evidence of the general propensity for rocks to granularly disaggregate [*Eppes and Griffing*, 2010; *Gómez-Heras et al.*, 2006; *Goudie*, 2013; *Siegesmund et al.*, 2000]. Thus, our modeling is limited to one—albeit common—style of rock cracking, granular disaggregation (Figure 2a).
4. We use order of magnitude calculations to address the growth of cracks from their initial lengths to their critical lengths. Such an approach is desirable given the innate heterogeneity of geologic materials. Then, noting that such an approach dictates that subtracting two values of the same order of magnitude yields the same order of magnitude, we estimate that the characteristic distance of growth from a crack's incipient to critical length is the average grain size of the rock, d_g.
5. We assume that modeled cracks are not growing along some inherent heterogeneity such as foliation, which would influence K. As such, any in-growing crack lying at a given depth, z, will tend to arrest at depths on the order of $z + d_g$, due to impingement on grains of differing strength or orientations at the lower depth. Crack growth arrest due to impingement on nearby grains is commonly observed in experimental data [e.g., *Swanson*, 1984].
6. We assume that stresses are largest at the rock surface. This assumption likely holds for many environmental stresses. In the case of thermal stresses considered here, this assumption follows from the fact that characteristic grain dimensions, d_g, are much smaller than the characteristic diurnal thermal penetration depth, δ_T, which our estimates show is on the order of ~25 cm for granites with generic properties (Appendix C). For processes like salt growth and freezing, current understanding [*Hales and Roering*, 2007; *McAllister et al.*, 2017] suggests that grain size is likewise much smaller than the characteristic depth of penetration of liquid water and freeze zones.
7. For cracks having characteristic lengths on the order of d_g, we assume that associated zones of both thermal or stress intensity influence are likewise on the order of d_g. In other words, adjacent cracks found ~d_g distance away do not influence either the thermal stress or the stress intensity of the crack being modeled.
8. In terms of the intergranular thermal stresses considered here, we consider granite to be composed of two primary constituent minerals, feldspar and quartz (Appendix C). A recent numerical model suggests that these minerals dominate the thermal stress and fracture response of granite [*Vázquez et al.*, 2015].
9. We assume that thermal stresses within the region of the modeled crack remain oriented roughly parallel to the rock surface [*Shi*, 2011], so that grain layers within this high-stress zone experience roughly cyclic compressive and tensile, surface-tangential loads. Thus, we assume that cracks grow predominantly in a direction normal to the rock surface. This assumption is supported by field observations showing that a majority of surface cracks in boulders exhibit subvertical to vertical dip angles [*Aldred et al.*, 2015].

We reemphasize that we focus on the simplest case wherein thermal stresses are produced solely by diurnal temperature cycling and subcritical cracking occurs only at grain boundaries over relatively short spatial scales before critical cracking occurs. In addition, our model does not account for the effects of thermal cycling over longer or shorter timescales. Nor does it consider rock albedo [*Gómez-Heras et al.*, 2006; *Hall et al.*, 2005; *Viles*, 2005; *Warke and Smith*, 1998], biologic cover [*Mayaud et al.*, 2014], light penetration [*Hall et al.*, 2010], or rapid temperature fluctuations associated with weather [*McKay et al.*, 2009; *Smith et al.*, 2011]; all of which can impact the magnitude, as well as the phase of thermal stresses, i.e., the timing of diurnal temperature peaks and troughs. Similarly, we do not account for rock geometric effects where, for

example, thermally induced subsurface temperatures and stresses can arise within individual boulders or rock outcrops due to rock shape [*Eppes et al.*, 2016; *Molaro et al.*, 2017; *Shi*, 2011]. Likewise, the model neglects thermal expansion anisotropy along different mineral axes, which can be large, e.g., in calcite or feldspar [*Fei*, 1995], and strongly influence subcritical cracking due to thermal stress [*Meredith et al.*, 2001].

4.2. Model Development

In order to determine cyclic, thermally driven, subcritical cracking, we must integrate equation (1). Integration requires, in turn, information on stress- and moisture-dependent parameters.

Readers not interested in the technical details associated with the subcritical cracking model derivation may skip to section 5.

4.2.1. Accommodation of Stress

Considering the stress intensity amplitude, ΔK_I (equation (1)), for surface cracks growing into a planar, effectively semi-infinite region, fracture mechanics [*Anderson*, 2005] gives ΔK_I as

$$\Delta K_I = \Delta K_I(z,t) = \Delta\sigma_{\max,\text{eff}}\sqrt{\pi a(z,t)} \tag{2}$$

where $\Delta K_I(z,\mathrm{t})$ and $a(z,t)$ are, respectively, the time- and depth-dependent stress intensity amplitude and crack length. In the case of this work, the effective stress amplitude comes from intergranular thermal stress arising in a rock exposed to diurnal temperature cycling and having two primary mineral constituents with different coefficients of thermal expansion (Appendix C; equation (C7)):

$$\Delta\sigma_{\max} = \Delta\alpha E\Delta T_o/(1-\nu) \tag{3}$$

Here $\Delta T_o = T_{\text{surface,max}} - T_\infty$ is the maximum surface temperature variation produced by diurnal temperature cycling, $\Delta\alpha$ = the difference in the coefficients of thermal expansion of the mineral constituents, E = Young's modulus, and ν = Poisson's ratio.

Equation (3) neglects the depth-wise decay in the near-surface temperature field, at least over length scales on the order of in-growing cracks. We assume, however, that time-varying temperatures within the near-surface crack zone essentially track with, and have the same magnitude as, the time-varying rock surface temperature. This assumption is valid (1) because we are only considering cracks on the order of the characteristic grain size, d_g (Appendix C), and (2) because d_g for typical granite as well as for virtually all rock types will be much smaller than the thermal penetration depth, δ_T. Thus, we use ΔT_o when calculating both the maximum characteristic stress, $\Delta\sigma_{\max}$, in equation (3) and the associated stress intensity amplitude, ΔK_I, in equation (2).

4.2.2. Accommodation of Moisture

As previously mentioned, almost no data exist on m and C, the Paris law exponent and coefficient for cyclic fatigue cracking of rock under different environmental conditions. However, some experimental data *have been* gathered on *noncyclic* environmentally dependent subcritical cracking of rocks. These data are generally correlated using Charles' law [*Charles*, 1958] of subcritical crack growth:

$$\frac{da}{dt} = C_c K_I^n \tag{4}$$

where the left-hand side is the crack growth rate; C_c is a rock- and climate-dependent constant; K_I is the stress- and crack-geometry-dependent stress intensity; and n is the rock- *and* environment-dependent "subcritical crack growth index." (The parameter n is often also referred to as the "stress corrosion index," a misnomer since subcritical cracking proceeds by any number of processes including stress corrosion (section 2.1.1).)

Because cracking is predicated on chemical reactions (Figure 1; section 2.2.3), n is strongly dependent on the amount of moisture present during testing, either in the form of ambient humidity or surface water (e.g., reviews in *Atkinson* [1987] and *Brantut et al.* [2013]). We therefore—after demonstrating $m = n$ (Appendix A)—incorporate existing empirical data [*Nara et al.*, 2013] relating n to ambient humidity conditions for granitic rocks into our crack growth model (section 7). Although we employ only a single suite of measured n-moisture relationships in our calculations, experimental data show that similar climate sensitivity appears to exist in n for most rock types (e.g., *Nara and Kaneko* [2006], *Nara et al.* [2013], and *Nara et al.* [2011]).

4.2.3. Crack Evolution per Stress Cycle

Considering a single, surface-initiated, representative crack, growing under cyclic heating, in a rock that remains fixed at a given location, we integrate equation (1), obtaining a relationship that describes the length of the representative crack, $a(N)$, following N cycles of diurnal heating:

$$a(N) = \left[a_o^{\beta} + \beta C_1 N\right]^{1/\beta} \tag{5}$$

Here a_o is the intial crack length, $\beta = 1 - m/2$, $C_1 = C\ \Delta\sigma_{\max}^{m}\pi^{m/2}$, and $\Delta\sigma_{\max}$ is given by equation (3). Equation (5) provides the basis for derivation of a simplified but equivalent and physically transparent crack growth equation (section 7).

5. Derivation of Model Input Parameters Specific to and Necessary for Predicting Climate-Dependent Subcritical Cracking in a Weathering Environment

As we have described above, most research on subcritical cracking in rock has been conducted in the context of tectonically driven fracture of relatively deep crustal rocks. Thus, gaps in the existing characterization of subcritical cracking must be addressed in order to use our predictive rock cracking and rock erosion rate models in the context of weathering conditions.

In Appendix A, we provide details of our determination of the equivalence between the Paris' law and Charles' law exponents m and n, respectively. In brief, we consider an idealized experiment in which a large set, N, of nominally identical stress relaxation tests, performed on N separate, nominally identical rock specimens, is performed (Figure A1). An (ensemble) average, time-dependent stress relaxation, $<\sigma(t)>$, can then be determined (over the set of N specimens). Repeating this experiment an infinite number of times, using separate sets of N nominally identical rock specimens in each experiment then allows construction of an infinitely long, repeating cycle of ensemble averaged stress relation histories. Performing a Fourier decomposition of the latter finally allows us to interpret the infinite series of ensemble averaged stress relaxation histories as an equivalent superposition of purely sinusoidal, infinite-in-time load histories, showing that $m = n$.

In Appendix D, we derive and validate—against measured values from two different materials—an estimate for the Paris' law coefficient:

$$C \sim d_g K_c^{-m} \tag{6}$$

where d_g is the rock characteristic rock grain size, K_c the rock fracture toughness, and m is the Paris law exponent.

In Appendix E, we derive and validate—against measured values in rock—an approximate, common material property-dependent relationship for the threshold stress intensity, K_{th}, required for initiation of subcritical crack growth (see section 2.2.8 for background):

$$K_{\text{th}} \sim \sigma_T \sqrt{d_g} \tag{7}$$

where σ_T is the rock tensile strength and d_g is the characteristic rock grain size.

It should be noted that we do not evaluate the extent to which our estimations of any of these parameters might be applicable to subcritical cracking at scales greater than grain scale.

6. Subcritical Cracking Model Validation

We test the proposed subcritical cracking model (equation (5)) against *observed* short timescale crack evolutions, as well as *predicted* long timescale evolutions, as reported by *Delbo et al.* [2014] for two asteroid rock types exposed to experimentally controlled cyclic heating.

Based on the rock thermal and thermoelastic properties for the rock types given in *Delbo et al.* [2014], we assume the following parameter values: $m = 3.86$, $\Delta T_o = 190$ K, $\alpha = 8.5 \times 10^{-6}\text{K}^{-1}$, $C = 3 \times 10^{-4}$ m $[\text{MPa}\sqrt{m}]^{-n}$, E_{oc}=56×10^{3}MPa, E_{cc}=29×10^{3}MPa, and $\nu = 0.11$. Here $\alpha = \chi\alpha_i + (1-\chi)\alpha_m$ is the bulk thermal expansion coefficient, α_i and α_m are chondrule and matrix thermal expansion coefficients, χ and $(1-\chi)$ are

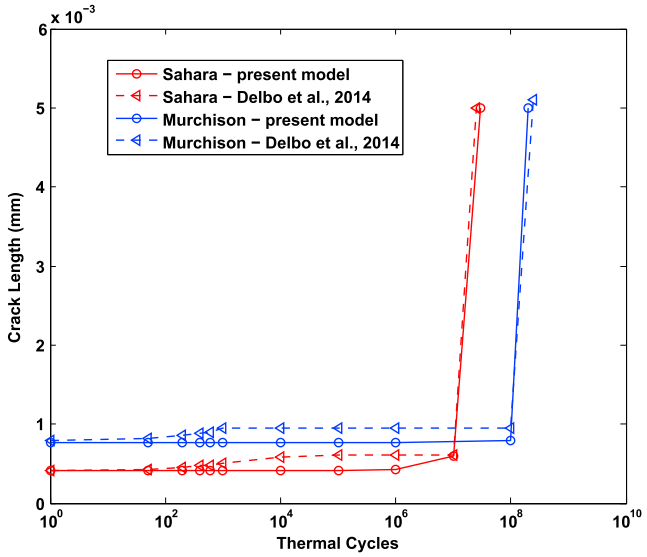

Figure 3. Subcritical cracking model validation results. Our calculations of subcritical cracking due to diurnal thermal stresses are compared to results from those observed and calculated in *Delbo et al.* [2014] for ordinary (Sahara) and carbonaceous (Murchison) chondrites. Units on the *x* axis are the time-equivalent to a single "day" of a rotating asteroid as detailed by *Delbo et al.* [2014].

corresponding volume fractions, C is the Paris law coefficient, and E_{oc} and E_{cc} are the bulk moduli for ordinary and carbonaceous chondrite, respectively. Due to lack of data, the value for the Poisson ratio, ν, is assumed to be approximately equal to that for granite, $\nu = 0.22$, and is taken as the intermediate value of the range (0.1–0.33) reported in *Gercek* [2007]. Initial crack sizes are taken from *Delbo et al.* [2014].

Since chondrites are composed of chondrules embedded in a fine-grained matrix, we define the difference in constituent thermal expansion coefficients as $\Delta\alpha = \alpha_i - \alpha_m$, where, from *Delbo et al.* [2014], $\alpha_i = 10.4 \times 10^{-6}\mathrm{K}^{-1}$. Unfortunately, no data apparently exist on characteristic thermal expansion coefficients for typical matrix materials, α_m, and no information is given in *Delbo et al.* [2014] on chondrule and matrix volume fractions. Thus, for purposes of model validation, a rough estimate of α_m is obtained by an inverse procedure: (a) values of α_m are iteratively varied until predicted lifetimes for *ordinary chondrite* (*Sahara*), as obtained by the present model, approximately match those obtained by the model in *Delbo et al.*, and (b) the value of α_m thus obtained, $\alpha_m = 8.17 \times 10^{-6}\mathrm{K}^{-1}$, is then used to predict lifetimes for *carbonaceous chondrite* (*Murchison*) and again compared against the prediction from *Delbo et al.* [2014].

Crack lifetimes, or equivalently, approximate chondrite lifetimes predicted by the present model, are compared in Figure 3 against those predicted by the two-scale model in *Delbo et al.* [2014]. As shown, reasonable agreement is observed for both ordinary and carbonaceous rock types. It is important to note, however, that predicted crack lifetimes are sensitive to the parameters m and C, as well as $\Delta\alpha$. *Delbo et al.* [2014] considers the effects of uncertainty in m and C on predicted crack evolutions. Here with regard to $\Delta\alpha$, we find that over the short ~1000 h experimental timescales used in *Delbo et al.* [2014], crack evolutions predicted by the present model are fully consistent with observed evolutions and are largely insensitive to $\Delta\alpha$, at least over the range $10^{-3}\alpha \le \Delta\alpha \le 10^{-1}\alpha$. By contrast, for the same range of $\Delta\alpha$, predicted crack lifetimes over long timescales, 10^3 to 10^7 thermal cycles [*Delbo et al.*, 2014], vary by orders of magnitude.

Nevertheless, using the parameters given above, as well as the value of $\Delta\alpha = \alpha_i - \alpha_m = 2.55 \times 10^{-6}\mathrm{K}^{-1}$, obtained as described above, we find reasonable agreement between crack evolutions predicted by the simple model in equation (5) and both short timescale experimental observations in *Delbo et al.* [2014] and long timescale predictions obtained via *Delbo*'s relatively complex two-scale model [*Delbo et al.*, 2014]. These results (i) support the validity of our simple crack model, equation (5), and (ii) provide further support for the ansatz, $\Delta\alpha = \alpha_1 - \alpha_2$, proposed in equation (C5) of Appendix C.

7. Evaluating the Effects of Climate on Subcritical Cracking

7.1. Incorporating Realistic Data Into the Proposed Subcritical Cracking Model

In order to expose climatic effects on subcritical cracking (in this case specifically, the effects of long timescale mean relative humidity, $\langle \mathrm{RH} \rangle$, and long timescale mean diurnal temperature range, $\langle \Delta T \rangle$), we recast equation (5) in an approximate form that highlights these dependencies by enabling the use of realistic moisture and temperature data and produces crack growth rates:

$$N = N(\langle \mathrm{RH} \rangle, \langle \Delta T \rangle) \sim [m(\langle \mathrm{RH} \rangle)/2 - 1]^{-1} [K_c / \Delta K_I(\langle \Delta T \rangle)]^{m(\langle \mathrm{RH} \rangle)} \quad (8)$$

Here $N(\langle \mathrm{RH} \rangle, \langle \Delta T \rangle)$ is the approximate minimum number of days required for an incipient, near-surface, subgrain-scale crack to grow from incipience to a critical length, a_c, which is on the order of size of d_g (Appendix D). The effect of humidity on the subcritical crack growth index, n, is captured by the empirical correlation between n and relative humidity (RH) taken from *Nara et al.* [2013] and by the equivalence of n with m, the Paris law exponent (Appendix A). Finally, the relationship between the average diurnal stress intensity fluctuation, ΔK_I, and the mean annual rock-surface temperature variation, $\langle \Delta T \rangle$, is captured using

$$\Delta K_I(\langle \Delta T \rangle) = [\Delta\alpha \langle \Delta T \rangle E/(1-\nu)]\sqrt{\pi d_g} \tag{9}$$

where $\langle \Delta T \rangle = \langle |T_{\max} - T_{\min}| \rangle$ is the annual average of the daily temperature variation of the rock surface (and where $T_{\max} - T_{\min}$ can, in extreme climates, be negative).

We present cracking rates as the minimum time required, $\tau_{c,\min}$, for a near-surface crack to grow subcritically from incipience to a critical length, $a_c \sim d_g$:

$$\tau_{c,\min} = N(\langle \mathrm{RH} \rangle, \langle \Delta T \rangle) \tag{10}$$

This approach (i) provides a lower bound on moisture- and temperature-sensitive, near-surface subcritical cracking and (ii) exposes the influence of these climate parameters on subcritical cracking.

Equation (8) is derived as follows:

1. Let N_{tot} represent the number of diurnal heating cycles that a representative crack experiences as it grows from an initial length of a_o, on or near an exposed rock surface, to a final length of a_c. Setting $a(N) = a(N_{\mathrm{tot}}) = a_c$ and $N = N_{\mathrm{tot}}$ in equation (5) and solving for N_{tot} then yields

$$N_{\mathrm{tot}} = \left[a_o^{-\psi} - a_c^{-\psi}\right][\psi C_1]^{-1} \tag{11}$$

where $\psi = -\beta = m/2 - 1$, $C_1 = C(m)\,\Delta\sigma_{\max}^m \pi^{m/2} = C(m)[\,\Delta\alpha\langle\,\Delta T_o\rangle E/(1-\nu)]\sqrt{\pi d_g}$.
2. We use equation (D3), $C \sim d_g K_c^{-m}$, from Appendix D to approximate the Paris law coefficient.
3. Given the natural heterogeneity in rock, we treat the growth of the crack from a_o to a_c using an order of magnitude analysis. As previously mentioned, both are assumed to be of a size on the same order of magnitude of d_g. Using equation (11), and noting that subtracting two terms of the same order of magnitude, $a_o^{-\psi} - a_c^{-\psi} \sim O\left(d_g^{-\psi}\right) - O\left(d_g^{-\psi}\right) = O\left(d_g^{-\psi}\right)$, yields a difference having the same order of magnitude, we obtain the approximate expression in equation (9).

7.2. Calculating Climate-Dependent Subcritical Cracking Under Generic Stress

In general, analytical models [e.g., *Costin and Holcomb*, 1981] indicate that rates of subcritical cracking under cyclic loads, regardless of the load origin, increase as the amplitude of the stress intensity, ΔK_I, approaches a critical magnitude related to the fracture toughness K_c. With this effect in mind, we can restate equation (8) in a generic form connecting the number of diurnal, subgrain- and grain-scale, near-surface subcritical crack events experienced by the rock, $N = \tau_{c,\min}$, to a ratio, $\Delta K_I/K_c$. This ratio juxtaposes the amplitude of the characteristic diurnal stress intensity variation relative to the rock's fracture toughness:

$$N = \tau_{c,\min} = \tau_{c,\min}(\langle \mathrm{RH} \rangle, \Delta K_I/K_c) \sim [\Delta K_I/K_c]^{-m(\langle \mathrm{RH} \rangle)}\,[m(\langle \mathrm{RH} \rangle)/2 - 1]^{-1} \tag{12}$$

where again, $m(\langle \mathrm{RH} \rangle) = m_0 - m_1 \times \langle \mathrm{RH} \rangle$.

Considering stress as a ratio in this way makes the model results quantitatively applicable to any source of stress whose magnitude is lower than the fracture toughness, K_c, employed in the calculations (Table 1). Thus, the remainder of section 7 is focused on combining equation (9) with equation (10) to calculate $\tau_{c,\min}$ as a function of the single climate variable relative humidity $\langle RH \rangle$.

Specific assumptions to this approach are as follows:

1. The crack growth equation, equation (3) or its equivalent, equation (8), assumes fixed m and C through time—likely an oversimplification. Nevertheless, since both of these parameters depend on relative humidity, we also fix RH at a long-time average, $\langle \mathrm{RH} \rangle$.
2. Time averages must be obtained over periods that meet or exceed the characteristic time, τ_c, required for a representative crack to grow from a_o to a_c. Thus, we do not take into account climate change during model runs.

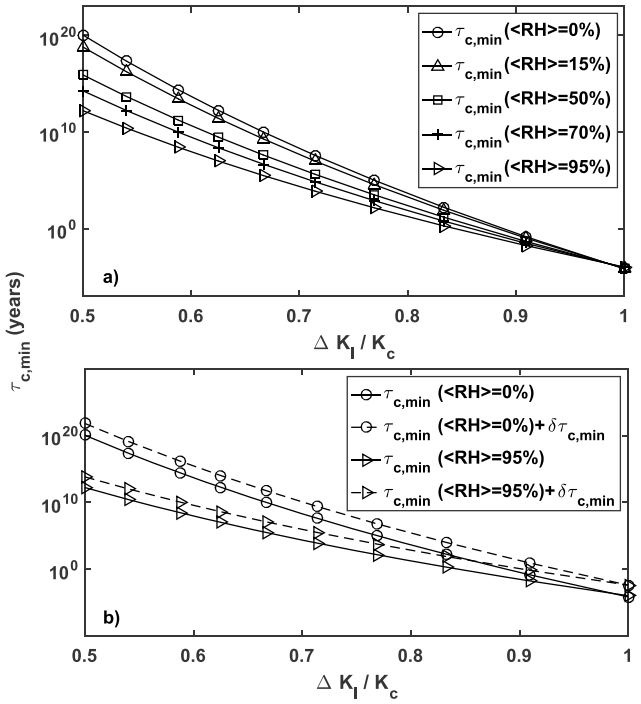

Figure 4. (a) The minimum time required, $\tau_{c,min}$, for a representative, surface- or near-surface crack to grow to a critical length in a rock having parameters listed in Table 1 and plotted as a function of the experienced stress intensity amplitude relative to rock fracture toughness, $\Delta K_I/K_c$, and the long-time average relative humidity, $\langle RH \rangle$. Thus, here—by considering stress as a ratio to fracture toughness—$\tau_{c,min}$ is calculated and plotted as a function of *any* generic, environment-driven, nominally diurnal, seasonal, *or* random source of near-surface tensile stress. (b) The potential variability, $\delta\tau_{c,min}$, in minimum crack lifetimes, $\tau_{c,min}$, estimated using equation (13) and the general range of known values of different rock parameters. Based on available data, we assume that $\delta K_c/K_c \sim 0.5$ and that $\delta(\Delta K_I)/\Delta K_I \sim 0.5$. Additionally, focusing on Westerly granite, an estimate for the mean, humidity-dependent Paris law/Charles' law exponent, m/n, is obtained using *Nara et al.* [2013]: $m = m_o - m_1 \times \langle RH \rangle$, where again, $m_o = 80.4$ and $m_1 = 0.28$. Due to the magnifying effect of large m on the relative variabilities, $\delta K_c/K_c$ and $\delta(\Delta K_I)/\Delta K_I$, in equation (13), even small and moderate relative variabilities in the latter produce large estimated relative variability in $\delta\tau_{c,min}/\tau_{c,min}$. For this reason, $\tau_{c,min} - \delta\tau_{c,min}$, is, for all $\Delta K_I/K_c$ shown, negative and is thus not presented. The implication of this sensitivity analysis is that cracking velocity—under many combinations of these parameters—ranges significantly; the relative influence of humidity, however, does not. (Note: in the case of a repeating, nominally seasonal stress, a conversion factor, c = (1 season)/(average days per season), multiplies the right side of equation (12). Further, the case of a randomly acting environmental stress (es) would require determination of an average time-varying stress history, followed by Fourier decomposition of the history, with equation (12) applied to each Fourier stress mode. Treatment of the random case would follow the linear damage model [*Anderson*, 2005]).

7.2.1. Results

Our calculations demonstrate that for any given generically sourced stress magnitude, there are accelerations in subcritical cracking—relative to water-free conditions—produced at even very low-average annual relative humidity (Figure 4a). As stress intensities experienced by the rock approach its fracture toughness, crack velocities increase, while the effects of moisture decrease. This relationship arises because chemical processes at crack tips are less efficacious when there is insufficient time for them to occur and/or moisture does not have time to transfer into the crack tip as it extends [*Atkinson*, 1987]. Thus, the influence of moisture becomes less apparent under relatively high ΔK_I.

Nevertheless, the influence of humidity will remain as shown even when several tensile stress-loading mechanisms are acting on the rock at the same time. In other words, humidity, regardless of the sequence and magnitudes of daily stress, amplifies the summed effect of *all* weathering-related stress loading processes. This conclusion is mathematically valid assuming (a) that the weathering-related tensile stresses act as superposed, noninteracting (i.e., linear) processes; (b) that grain-scale crack healing processes remain negligible; and (c) that the daily effect of these randomly imposed weathering-related processes results in an approximately fixed daily variation in the stress intensity factor, ΔK_I,

Further—for any given long-time average relative humidity—subcritical cracking rates exhibit a clear sigmoid character, with rapid, accelerating growth occurring as the stress intensity, ΔK_I, begins to approach K_c (Figure 4). For any given crack, this effect physically corresponds to an often long period of very slow subcritical crack growth, which gradually transitions—as crack lengths approaches the critical length—to relatively fast growth. Thus, our results demonstrate how long periods of slow subcritical cracking, under low stress intensity, can lead to critical cracking without any substantial change in stress-loading magnitude.

7.2.2. Model Result Variability Due to Rock and Environment Variabilities

The results depicted in Figure 4a are calculated using an average value of K_c and a single set of data quantifying the relationship between the subcritical crack growth index, n, and humidity for granite. In

reality, however, due to natural variability in rock composition—and geologic and climatic history—all of the fracture mechanics properties employed to make those calculations, not just n, will change in both time and space. Therefore, in Appendix F, we outline a generic method for estimating variability in $\tau_{c,\min}$ produced by random, natural variations in K_c, ΔK_I, and n. In the case of weathering, natural variability arises from two sources: (i) variability, over many time scales, in climate, and (ii) variability in rock material properties, the latter determined by numerous factors including rock mineralogy, microstructure, and both chemical and physical weathering history.

A standard propagation of uncertainty argument [*Coleman and Steele*, 2009] leads to the following expression for estimating the band of variability in minimum crack lifetime estimates (detailed in Appendix F):

$$\left(\frac{\delta\tau_{c,\min}}{\tau_{c,\min}}\right)=\sqrt{(n(\langle \mathrm{RH}\rangle))^2\left(\frac{\delta K_c}{K_c}\right)^2+(n(\langle \mathrm{RH}\rangle))^2\left(\frac{\delta(\Delta K_I)}{(\Delta K_I)}\right)^2+\left[\ln\left(\tau_{c,\min}\right)-n^{-1}\right]^2\left(\frac{\delta n}{n}\right)^2} \tag{13}$$

Here $\delta\tau_{c,\min}/\tau_{c,\min}$ is the estimated relative variability in $\tau_{c,\min}$, as produced by known or, more typically, estimated relative variabilities, $\delta K_c/K_c$, $\delta(\Delta K_I)/\Delta K_I$, and $\delta n/n$, in K_c, ΔK_I, and n, respectively.

In equation (13), mean values of $\tau_{c,\min}$, K_c, ΔK_I, and n are used wherever these variables appear without a leading δ. In addition, the strong dependence of n on the climate-dependent average humidity, $\langle \mathrm{RH}\rangle$, is emphasized, and we formulate the equation to accommodate any source of stress. In order to estimate the relative variabilities, $\delta K_c/K_c$ and $\delta n/n$, we suggest that for any given family of similar rock types, available measurements of K_c and m be pooled and used as follows: (i) rough estimates of mean K_c and moisture-dependent mean $n=n(\langle \mathrm{RH}\rangle)$ should first be determined. (ii) Observed spreads, $K_{c,\max}-K_{c,\min}$ and $n_{\max}(\langle \mathrm{RH}\rangle)-n(\langle \mathrm{RH}\rangle)$, in available data can then be used as rough surrogates for δK_c and δn.

The results of this estimate for $\delta\tau_{c,\min}$, shown as a function of average relative humidity, $\langle \mathrm{RH}\rangle$, are presented in Figure 4b with details of the calculations provided in section F4. For clarity, we show only the estimated variability bands corresponding to the largest and smallest relative humidity, $\langle \mathrm{RH}\rangle=95\%$ and $\langle \mathrm{RH}\rangle=0\%$, respectively, presented in Figure 4a.

As illustrated by equation (13), the estimated variability in $\tau_{c,\min}$ is strongly sensitive to the magnitude of the subcritical crack growth index, n. In rocks like granite, where n can exceed 10^2 [*Meredith and Atkinson*, 1985], it thus becomes apparent that even in cases where sufficient, high-quality data are available to find well-constrained estimates of $\delta K_c/K_c$ and $\delta(\Delta K_I)/\Delta K_I$; large Paris law exponents magnify these, resulting in significant variability in estimated crack lifetimes, $\tau_{c,\min}$. (Note that the lower bounding values of $\tau_{c,\min}$ are not depicted because they fall below 0.) Thus, this sensitivity analysis demonstrates that subcritical cracking rates vary drastically within the limits of known rock parameters, making the case for a critical need of their accurate measurement. Regardless of the variability, however, the acceleration in cracking due to humidity—for a given stress/critical stress ratio—remains.

8. A Simple Model of Rock Erosion by Climate-Dependent Subcritical Cracking

In order to translate climate-dependent subcritical cracking rates into terms more readily understood in the context of Earth surface processes, we present an approximate model of in situ rock erosion driven by subcritical cracking. Weathering is idealized, whereby, over time, small surface and near-surface intergranular cracks grow due *solely* to intergranular thermal stresses. We employ the approach described in sections 4–7, whereby we only consider grain-scale intergranular cracking, ignoring that the surfaces of most rocks in all environments are characterized by common flaws that are greater in length than the average grain size [*Adelsberger and Smith*, 2009; *Aldred et al.*, 2015; *Eppes et al.*, 2010].

In the model, subgrain-scale cracks subcritically grow to critical lengths—on the order of the rock's characteristic grain size—whereupon critical cracking occurs. We assume that at this point the rock's outermost surface, having a thickness equal to the grain size, exfoliates (spalls) or granularly disaggregates. We propose a hypothesis that as far as we know has not been previously stated: that such exfoliation or disaggregation is driven, at least in part, by the comparatively large energy release that accompanies critical cracking. Afterward, a relatively unweathered surface is exposed, a new crack begins subcritically propagating, and the process repeats.

Our rock erosion framework is supported by a number of experimental and field observations, as well as by theoretical studies:

1. Even over relatively short (Holocene) timescales, regardless of rock type or environment, the outer millimeter to centimeter thick portion of rock surfaces is characterized by chemically and physically altered weathering rinds that thicken and intensify in their accumulation of weathering products through time [*Birkeland*, 1982; *Burke and Birkeland*, 1979; *Hoke and Turcotte*, 2002; *Warke and Smith*, 2000]. Accumulation of weathering products presumably "primes" this outer shell for wholesale exfoliation and/or susceptibility to thermal stresses, as proposed by some work [*Lamp et al.*, 2017; *Tratebas et al.*, 2004].
2. A large majority of all subaerially exposed rocks show evidence of this type of surface parallel fracturing and/or granular disintegration regardless of environment and/or stress loading process. For example, freezing, fire, salt hydration, and thermal cycling have all been demonstrated to induce exfoliation [e.g., *Al-Omari et al.*, 2014; *Turkington and Paradise*, 2005; *Vasile and Vespremeanu-Stroe*, 2016], and such spallation occurs in subsurface rock weathering as well [*Fletcher and Brantley*, 2010].
3. Similar surface fragmentation models have been explored and validated, for example, in the context of dissolution weathering rinds [*Hoke and Turcotte*, 2002] or salt weathering [*Wells et al.*, 2008].

Thus, although throughgoing cracking certainly and commonly plays a role in overall rock weathering [e.g., *Mushkin et al.*, 2014], small-scale spalling and/or granular disaggredation—due to its apparent prevalence in all environments and rock types—represents a reasonable model for approximating rock erosion, regardless of the source of stress.

8.1. Rock Erosion Model Assumptions and Idealizations

Additional assumptions and simplifications, as well a few explanatory notes, are as follows:

1. We idealize the relationship between daily variations in RH and ΔT (equations (3) and (8)) and assume that at least over long timescales—on the order of a year or more—these processes are uncorrelated.
2. The number of subcritical cracking events required for crack growth from lengths of a_0 to a_c, $N = N(\langle \mathrm{RH} \rangle, \langle \Delta T \rangle)$ in equation (8) thus represents an *average*, observed over the same period used to determine the average climate, i.e., $\langle \mathrm{RH} \rangle$ and $\langle \Delta T \rangle$.
3. For simplicity, the model applies to flat bedrock in which a representative crack, having an initial length on the order of the average grain size, d_g, grows strictly perpendicular to the planar rock surface. The model remains valid for individual rock clasts—like a boulder—under the fairly nonrestrictive condition that the ratio of critical crack length to characteristic rock radius R is small, $a_c/R \ll 1$.
4. In light of the physical picture that a near-surface, high-stress region emerges at the top of the rock, we assume that the exposed near-surface layer remains intact—even as cracks grow into it—in the sense that tangential thermal stresses continue to be transmitted as if the layer were a homogeneous, fixed property region. Since we have already assumed that the zone of influence (on the surrounding stress field) of individual, grain-scale cracks is only on the order of d_g, this is a consistent assumption, even when the layer has a high density of grain-scale cracks.
5. The timescale for removal of the outermost, critically cracked rock layer, τ_E, is assumed to be short relative to the characteristic time, τ_G, required for the representative crack to grow from a_o to a_c and is therefore idealized as an instantaneous process. This assumed behavior suggests that grains within the high-stress layer, if not ejected during a critical cracking event, become significantly uncoupled from the surrounding rock matrix.
6. Given the importance of diurnal rock surface temperature range, ΔT, in subcritical cracking rates modeled here, in order to more realistically approximate annual variance in ΔT, rather than using average annual magnitudes, here we model the random distribution of daily temperature variations as Gaussian (Appendix G).
7. Because of the sensitivity of the magnitude of thermal stress to the difference in coefficients of thermal expansion of rock mineral constituents, $\Delta\alpha$, calculted rock erosion rates are also extremely sensitive to this parameter. We therefore perform erosion rate calculations over the full range of $\Delta\alpha$ between quartz and feldspar reported in commonly cited literature [*Fei*, 1995; *Robertson*, 1988; *Skinner*, 1966]: i.e., maximum reported α_quartz minus minimum reported α_feldspar ($\alpha_{\mathrm{quartz,max}} - \alpha_{\mathrm{feldspar,min}} = 5.06 \times 10^{-5}/°\mathrm{C}$) and minimum reported α_quartz minus maximum reported α_feldspar ($\alpha_{\mathrm{quartz,min}} - \alpha_{\mathrm{feldspar,max}} = 2.94 \times 10^{-5}/°\mathrm{C}$).

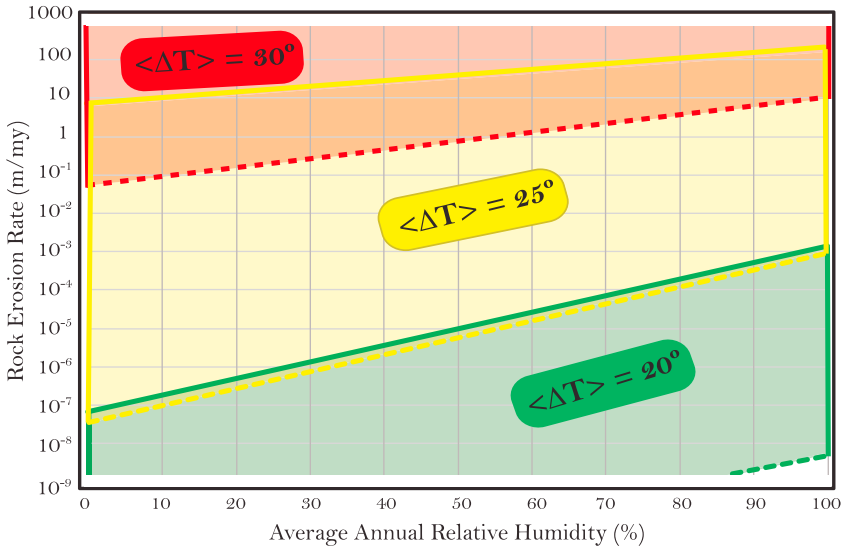

Figure 5. Modeled rock erosion rates driven by climate-dependent subcritical cracking, calculated for rocks with material properties presented in Table 1, experiencing only a single type of stress—intergranular thermal stresses due to diurnal temperature fluctuations—and only a single style of cracking—granular disaggregation. Grain-diameter thick layers erode from the rock after cracks subcritically propagate to those lengths. Each shaded region encompasses a range of erosion rates, calculated for each indicated average annual diurnal temperature range, as a function of climate-averaged relative humidity. The upper boundary of the boxes (solid lines) corresponds to high reported differences between constituent-mineral thermal expansion coefficients ($\alpha_{quartz,max} - \alpha_{feldspar,min} = 5.06 \times 10^{-5}$/°C), while lower boundary (dashed lines) corresponds to intermediate differences ($\alpha_{quartz,min} - \alpha_{feldspar,max} = 4.0 \times 10^{-5}$/°C; Table 1).

8. Similarly, we employ an average value for K_c (1.7 MPa m$^{1/2}$) derived from values reported for granite in Table 11.6 of *Atkinson* [1987] and an intermediate value of 0.22 for Poisson's ratio, v, as reported for granite in Figure 4 of *Gercek* [2007]. We note, however, that in the literature we reviewed, K_c magnitudes for granite typically range from 0.5 MPa m$^{1/2}$ [*Amaral et al.*, 2008] to 3.8 MPa m$^{1/2}$ (*Siren et al.* [2012]; beyond the above references, other studies include *Nara* [2010] and *Ouchterlony* [1990]). Poisson's ratio varies from ~0.1 to ~0.33 (review in *Gercek* [2007]).

8.2. Rock Erosion Rate Calculations

The estimated time required, $\tau_{life,}$ for thermal cycling-induced weathering to reduce rock from an initial characteristic size, R_o—roughly an equivalent initial radius of a boulder or outcrop—to a final equivalent radius, R_c, is given approximately by

$$\tau_{life} = \tau_{life}(\langle RH \rangle, \langle \Delta T \rangle; \Delta T_c) \approx (R_o - R_c) \times N(\langle RH \rangle, \langle \Delta T \rangle) / \left[f_{solar}(\Delta T_c) \times d_g \right] \quad (14)$$

Here $f_{solar}(\Delta T_c)$, given by equation (G3) in Appendix G, is the number of days per year that ΔT exceeds the rock-dependent critical threshold, ΔT_c, necessary for ΔK_I to approach K_c, and $N(\langle RH \rangle, \langle \Delta T \rangle)$, given by equation (8)), is the moisture- and temperature-dependent number of cracking events required for crack growth from a_o to a_c (section 7). The corresponding erosion rate, $\dot{L}$, then follows as

$$\dot{L} = (R_o - R_c)/\tau_{life} \quad (15)$$

8.3. Results

Using equations (14) and (15), combined with granite physical parameters from Table 1, we estimate erosion rates for granite rocks having a range of constituent mineral thermal properties (section 8.1), experiencing a full range of average annual relative humidity (0–100%) and experiencing three realistic values for annual average of daily rock surface temperature fluctuation. Figure 5 depicts the portion of these calculations that predict rock erosion rates greater than 10^{-9} m/Myr and less than 10^3 m/Myr, a range that well encompasses known and/or reasonable rates of rock erosion on Earth (see, e.g., the review in *Portenga and Bierman* [2011]).

Figure 5 schematically emphasizes that erosion rates driven by subcritical cracking depend strongly on moisture. Notably, at any given stress—as dictated by $\langle \Delta T \rangle$ combined with $\Delta\alpha$—erosion rates are as much as 4 orders of magnitude faster under high humidity, compared to zero humidity. These results also indicate that erosion driven by diurnal intergranular thermal stresses is strongly sensitive to the average diurnal temperature variation, $\langle \Delta T \rangle$, as well as differences in mineral constituent coefficients of thermal expansion, $\Delta\alpha$.

Erosion rates are also sensitive to the rock's fracture toughness, K_c, and Poisson's ratio (equation (3))—both of which are held constant for all calculations in Figure 5. As seen in Figure 4, subcritical cracking rates and therefore erosion rates will be extremely sensitive to K_c. Further, when the low end (0.1) of available reported values for Poisson's ratio for granite [*Gercek*, 2007] is employed instead of the intermediate value (0.22) used for Figure 5, calculated erosion rates are slower by 3–4 orders of magnitude for a given $\langle \Delta T \rangle$ and $\Delta\alpha$.

Finally, Figure 5 also illustrates that as overall stresses decrease, the influence of moisture on erosion rates becomes more pronounced, in a manner similar to that calculated for subcritical cracking (Figure 4). For example, at an average annual $\langle \Delta T \rangle$ of 20°C and a high $\Delta\alpha$, there is a ~2 order of magnitude increase in erosion rate between 50 and 100% humidity. However, at average annual $\langle \Delta T \rangle$ of 25°C and the same $\Delta\alpha$, that difference is reduced to <1 order of magnitude.

9. Discussion: Applicability and Limitations of the Modeling Results

We test the reasonableness of our rock erosion rate calculations, at least in a nullifying sense, by considering reported observations. Globally, erosion rates measured using analysis of in situ ^{10}Be, a cosmogenic radionuclide, for granite outcrops, range from ~10^{-1} to ~10^{2} m/Myr (e.g., review in *Portenga and Bierman* [2011]). Here calculated erosion rates (Figure 5) under climates and average annual rock temperatures similar to those measured in semiarid ($\langle RH \rangle \sim 37\%$; $\langle \Delta T \rangle \sim 31$°C) versus humid temperate locations ($\langle RH \rangle \sim 70\%$; $\langle \Delta T \rangle \sim 26$°C) [*Eppes et al.*, 2016, 2012] indicate that measurable erosion might be expected only for granites with very high values of Δa in the humid-temperate climate. It is not known what proportion of granites overall might be characterized by such values, presumably few. In the arid climates, more average granites—in terms of its mineral constituents' *a*—might experience significant erosion due to this one stress source. Field data suggest that active granular disaggredation, marked by loose crystals that can be brushed off, is common in granite outcrops and boulders located in semiarid landscapes. In contrast, granites exposed in humid temperate climates are typically marked by a polished or pitted appearance with no evidence of active subaerial grus formation [e.g., *Twidale and Romaní*, 2005].

The fact that our results suggest that erosion rates due solely to intergranular thermal stresses are effectively zero for most climate conditions and for most of the commonly observed range of rock properties is good support for the validity of the model itself. This one source of stress should not be sufficient to result in erosion rates comparable to those measured globally because all rocks experience many sources of stress.

Nevertheless, although intergranular thermal stresses, by themselves, may not typically result in significant long-term erosion, they likely ubiquitously and continuously contribute to the potential for "tipping the bucket" for subcritical cracking when other sources of tensile stress are superimposed on them or vice versa. For example, thermal stresses have been demonstrated to deform rock even at depths as great as 100 m when topographic stresses are at play [*Gischig et al.*, 2011a]. Similarly, acoustic emission-recorded subcritical cracking in boulders in temperate climates preferentially occurs when simple solar-induced diurnal thermal stresses coincide with other, weather-related ones [*Eppes et al.*, 2016].

Nevertheless our model predicts substantial erosion due to intergranular thermal stresses for rocks with large $\Delta\alpha$, experiencing relatively large $\langle \Delta T \rangle$, even under zero humidity. That any cracking at all would occur under 0% humidity follows from our assertion that both cyclic fatigue and environmentally assisted (as in Figure 1) subcritical cracking occur simultaneously. This is a reasonable assumption supported by the existing literature (section 2.2.3), and it allows for extrapolation of values of the subcritical crack growth index, *n*, through zero for our calculations. It should be noted, however, that little if any experimental data exist for subcritical cracking under zero humidity.

Further, in general, *n* is also strongly influenced by temperature (section 2.2.4). Thus, subcritical cracking velocity can be temperature—as it is manifest through climate—dependent even if the stress loading mechanism is not. In order to account for this feature, temperature- *and* moisture- dependent values of *n* and *C* would

need to be introduced into the model. Currently, however, analytical data addressing the *combined* effects of moisture and temperature for near surface, relatively low temperature conditions are also limited.

Our modeling does not address numerous additional complications and unknowns that arise in near surface environments. For example, the translation of moisture into voids for rocks in natural environments is poorly characterized (e.g., review in *Sass* [2005]) but likely complex [*McAllister et al.*, 2017], and numerous factors such as slope and slope aspect [e.g., *Burnett et al.*, 2008; *Langston et al.*, 2015; *Pelletier and Swetnam*, 2017] will influence that process. In turn, the presence of moisture will likely dampen thermal cycling and thus thermal stress. Further, weakening of the outer rock layer through development of either a weathering rind and/or surface-parallel fractures also likely plays critical roles in the tendency of outer layers to hold water or to crack [*Lamp et al.*, 2017].

When surface-parallel weaknesses are absent, there may be nothing to inhibit the subcritical growth of long, throughgoing cracks. The effect of these cracks on rock erosion rates and their evolution through time are likely complicated since they might, on the one hand, accelerate rock breakdown by increasing water advection and stress intensity (through the relationship, $\Delta K \propto \sqrt{a}$), while on the other, suppress thermal penetration into rock by acting as a thermal barrier.

In addition to environment-related complications that our modeling does not consider, there are also rock-related ones. For the thermal stresses considered here, mineral anisotropy with respect to coefficients of thermal expansion are known to play an important role in stress response to thermal cycling [*Widhalm et al.*, 1996]. Also, importantly, the rock parameters employed herein, including K_{th} and the subcritical crack growth index, n, will not only change with environmental conditions as we have shown but can also vary significantly even for a single general rock type like granite (see, for example, appendices in *Atkinson* [1987]). For example, microstructural complexity (poor sorting; high mineral heterogeneity) will lead to higher n values that can, in turn, influence density of cracking [*Atkinson*, 1984; *Olson*, 2004]. Further, although data from weathered rock are relatively limited, rock subcritical cracking parameters change as rocks weather and cracks grow [e.g., *Gupta and Rao*, 2000]. Thus, in order to accurately predict subcritical-cracking driven erosion in any given setting, rock parameters—as well as environmental conditions—must be well-characterized in the context of the location's surface and near-surface environmental conditions.

Finally, although the relationship between moisture and subcritical cracking that we explore herein is supported by published analytical data, there are other portions of our application of subcritical crack growth theory to the weathering and erosion problem that have not been tested with field or laboratory data. These include the $n = m$ equivalence (Appendix A), our estimation for C (Appendix D), and the long-term lower threshold of stress intensity, K_{th}, necessary for subcritical crack growth during granular disentigration (Appendix E).

Another untested feature concerns the competition that exists between depth-increasing confining pressure and depth-varying weathering stresses, such as those considered here (Appendix B). Although the inverse relationship between confining pressure and subcritical crack growth has been demonstrated under high confining pressures [e.g., *Brantut et al.*, 2014a; *Heap et al.*, 2011], there is currently no experimental data to support our theoretical conclusion of its influence at shallow depths. The interplay between these stresses and confining pressures is nevertheless important since they might, for example, provide a viable explanation for observed decreases in regolith production with increasing overburden thickness, as well as the so-called humped regolith production function [e.g., *Heimsath et al.*, 1997]. In these cases, the location of maximums in regolith production might represent some optimal depth at which surface-down stresses are maximized while confining pressure is minimized.

10. Summary and Conclusions

This paper presents a compendium of existing theory and data that elucidates how climate-dependent subcritical cracking is potentially a process by which most cracks grow in surface and near-surface rocks. Through our analysis, and by development of physically based models (sections 4–8), we expose several key features of subcritical cracking in the context of mechanical weathering and erosion.

Our analyses and modeling show that all weathering-related stress loading processes likely induce mechanical weathering through subcritical cracking, which itself is climate-dependent (Figures 4 and 5). For example,

our modeling results show that at any stress intensity lower than the rock fracture toughness, *linear* increases in climate-averaged relative humidity produce *exponential* increases in rates of subcritical cracking and associated rock erosion. This strong climate dependence of subcritical cracking arises through the chemophysical mechanism(s) by which atomic bonds are broken at crack tips when subcritical stresses are applied (Figure 1; section 2); published experimental data demonstrate that the general relationship likely holds for most common rock types (section 2).

Thus, rates of surface and near surface rock subcritical cracking by any source of stress, including tectonic and topographic, are likely climate-dependent, providing that such stresses exceed rock-specific threshold stress intensities, K_{th} (section 2.2.8). As stress intensities approach the fracture toughness, K_c, however, our modeling shows that subcritical cracking rates increase significantly, while the relative influence of moisture decreases (Figure 4).

Our modeling likewise indicates, however, the predominance of long periods of very slow crack growth in rocks characterized by flaws with subcritical lengths. These rocks would otherwise—under the low-magnitude stresses typical of weathering environments—lack sufficiently large flaws to induce significant cracking. In other words, even if weathering-related stresses occasionally approach or reach critical magnitudes, like through ground shaking [*Siman-Tov et al*., 2017] they are unlikely to have done so without prior sustained periods of subcritical cracking.

Similarly, as relatively unweathered rock that contains longer cracks (joints) or denser flaws (foliation or bedding) is exhumed, weathering rates might initially be large but then slow down as the rock adjusts—through subcritical cracking along these inherent weaknesses—to its new stress-loading conditions. We hypothesize that such a relationship might provide a mechanistic explanation for observations of faster regolith production rates in faster eroding landscapes [*Heimsath et al*., 2012], or initially fast, followed by slower, erosion after a climate change [*Garcin et al*., 2017].

Thus, commonly cited "physical weathering processes" (e.g., unloading, freezing, ice segregation, mineral hydration, crystal growth, and biologic processes) are more accurately, if not awkwardly, described as "weathering-related stress loading processes." Traditionally, mechanical weathering and geomorphology studies have focused on individual processes—freezing, thermal cycling, etc.—and accompanying environmental conditions—time in the "frost cracking window" or rates of temperature change, etc.—that cause such stresses [e.g., *Anderson*, 1998; *Hall and Thorn*, 2014; *McCabe et al*., 2007]. We conclude from fracture mechanics principles, however, that the mechanical weathering problem, at least between instances of large-scale/catastrophic critical cracking, can likely be considered *linear*. Therefore, all such sources of weathering-related stress are additive [*Anderson*, 2005] and can be superposed on each other as well as the diurnal thermal stresses modeled here.

To add further complexity, as cracks grow, rock weathers, and climate changes, the very rock parameters that dictate cracking velocity and/or stress—the subcritical crack growth index, fracture toughness, and Poisson's ratio—will also change (see discussion). Our modeling demonstrates that weathering and erosion rates are strongly sensitive to these parameters, as well as to small variations in rock surface and near-surface environment (e.g., Figure 4b). As such, this work highlights the critical importance of accurate measures of all of these factors.

Thus, we conclude that at large spatial scales, the relationship between climate and weathering, regolith production and erosion rates will also be complex and dependent on weathering and erosion history as well as microenvironmental conditions. These relationships represent a daunting and exciting new puzzle, motivated and limned by observations such as global rock erosion rates that are not strongly predicted by traditional climate metrics [e.g., *Portenga and Bierman*, 2011].

Finally, we note the development herein of several critical estimates for key fracture mechanics parameters. These estimates allow extension of available rock fracture and rock material property data to the ill-characterized problem of subcritical rock cracking under surface and near-surface conditions, and they will allow future workers to readily apply our approach, combined with existing data, to other rock types and stress conditions.

Overall, deciphering and quantifying the role that subcritical cracking may play in rock breakdown has key implications for workers seeking to explore the influence and feedbacks between climate, weathering, erosion, regolith production, and associated long-term landscape evolution. Our results demonstrate, for

example, that orders of magnitude of differences in erosion rate can be accounted for through differences in moisture alone, that is, without the influence of life or chemical weathering, both of which are often invoked to explain erosion-climate relationships [e.g., *Perron*, 2017]. Thus, if we seek to accurately define the driving or rate-limiting factors for Earth systems that involve weathering, we must better quantify the susceptibility of different rock types, under different environmental conditions, to subcritical cracking.

Appendix A: Equivalence of Charles Law and Paris Law Exponents, $m = n$

Consider an idealized ensemble of N rock samples, each of which is subjected to the same time varying, though noncyclic, experimentally controlled load history. Each rock sample is nominally identical; i.e., each is of the same nominal (bulk) mineral and chemical composition, the same spatial distributions of surface and subsurface water, and of the same shape and dimensions. Due to a consistent, grain-scale variability in the arrangement of constituent grains, however, the growth of initially identical, experimentally introduced surface cracks—one for each sample—is likewise spatially and temporally consistent.

For concreteness, consider Mode I, double torsion tensile loading, a typical rock failure experiment [*Atkinson and Meredith*, 1987], where the experimental load is quickly increased to near-critical magnitude and then, under fixed displacement conditions—and due to subcritical cracking—is allowed to relax. The ensemble of N load histories can be represented as a single quasiperiodic series of N cycles, each cycle consisting of a rapidly increasing load, followed by a slow, crack-induced decay. Due to the consistently variable grain-scale structure of each of the N samples, the load series representing the ensemble is not perfectly periodic, but rather exhibits cycle-to-cycle differences in maximum load and load evolution during both the initial loading period and subsequent load decay.

Next, replace the actual time series by its approximate mean equivalent, i.e.,

$$\langle \sigma(t) \rangle \approx \frac{1}{N} \sum_{j=1}^{N} \sigma_j(t) \tag{A1}$$

where $\sigma_j(t)$ is the measured stress evolution for the j^{th} sample, $0 \le t \le t_{\max}$, and $t_{\max}$ is the time span of the longest-lived load test. Now use the ensemble average stress evolution, $\langle \sigma(t) \rangle$, representing the average evolution over N tests, in Charles' law:

$$\frac{d\langle a \rangle}{dt} = C_c \langle K_I(t) \rangle^n = C_c \pi^{n/2} Y^n \langle \sigma(t) \rangle^n \langle a(t) \rangle^{n/2} \tag{A2}$$

where Y is a geometric parameter determined by the crack and load geometry [*Anderson*, 2005] and where we assume, due to random grain-scale structure, that the random, time-dependent load history, $\sigma(t)$, and the random crack-evolution, $a(t)$, are, at all times, t, statistically independent.

Equation (A2) can be interpreted as governing the evolution of a single hypothetical crack, during any one of N perfectly repeating load cycles, imposed on a single, idealized, hypothetical, though representative test sample. The sample is ideal since the crack formed during each load cycle closes at the end of the cycle, with the rock returning to its initial, preloaded state, a common crack modeling approach. An alternative interpretation is that equation (A2) describes the growth of a single representative—and again hypothetical crack—corresponding to the crack evolution of all N cracks in the ensemble, each evolution produced by the time-dependent load experienced by each of the N samples. Both views are rooted in and consistent with the statistical ensemble concept central to statistical mechanics [*Anderson*, 2005].

In order to connect crack growth data characterized by Charles' law to cyclic fatigue crack growth data described by Paris law, we exploit the first interpretation and expand the hypothetical, cyclic load, $\langle \sigma(t) \rangle$, in a Fourier series:

$$\langle \sigma(t) \rangle = \sum_{j=0}^{\infty} \sigma_{\text{cj}} \cos\frac{j\pi t}{T} + \sum_{k=1}^{\infty} \sigma_{\text{sk}} \sin\frac{k\pi t}{T} \tag{A3}$$

where $2T = t_{\max}$ and where the coefficients σ_{cj} and σ_{sk} are given by

$$\sigma_{\text{cj}} = \frac{1}{T} \int_0^{2T} \langle \sigma(t) \rangle \cos\frac{j\pi t}{T} dt$$

$$\sigma_{sk} = \frac{1}{T}\int_0^{2T} \langle \sigma(t) \rangle \sin\frac{k\pi t}{T} dt$$

Physically, equation (A3) suggests that application of the cyclic ensemble average stress, $\langle \sigma(t) \rangle$, to our single hypothetical rock sample is equivalent to applying, sequentially or simultaneously, an infinite set of sinusoidally varying stresses. (Note that the first applied stress in the first set of sinusoidal stresses, σ_{c0}, is actually constant.) Thus, the coefficients σ_{cj} and σ_{sk} in this picture represent the amplitudes of the j^{th} and k^{th} sinusoidal stresses.

We now adapt the classical linear damage model from fracture mechanics [e.g., *Anderson*, 2005] of cyclic fatigue crack growth to the present problem. Over the period of a single load cycle, t_{max} (again, associated with the perfectly periodic load, $\langle \sigma(t) \rangle$), we imagine that each of the sinusoidal loads, $\sigma_{cj} \cos\frac{j\pi t}{T}$ and $\sigma_{sk} \sin\frac{k\pi t}{T}$, in the two infinite sets of loads in equation (A3), is applied sequentially to the single, representative rock sample. Assume that the total change in crack length, δa, observed over a single period of the cycle, $0 \le t < t_{max}$—and produced by either $\langle \sigma(t) \rangle$, or equivalently, the infinite set of sequentially applied sinusoidal stresses in equation (A3)—remains much smaller than the crack length, a, observed at the beginning of the cycle, i.e., assume $\delta a/a \ll 1$. Based on this assumption, which is appropriate during subcritical growth under a wide range of experimental conditions, incremental crack lengths, δa_j and δa_k,produced by the j^{th} and k^{th} sinusoidal loads can be linearly superposed:

$$\delta a = \sum_{\beta=1}^{\infty} \delta a_\beta = \sum_{\beta=1}^{\infty} \left[\frac{\partial a}{\partial N}\right]_\beta N_\beta \tag{A4}$$

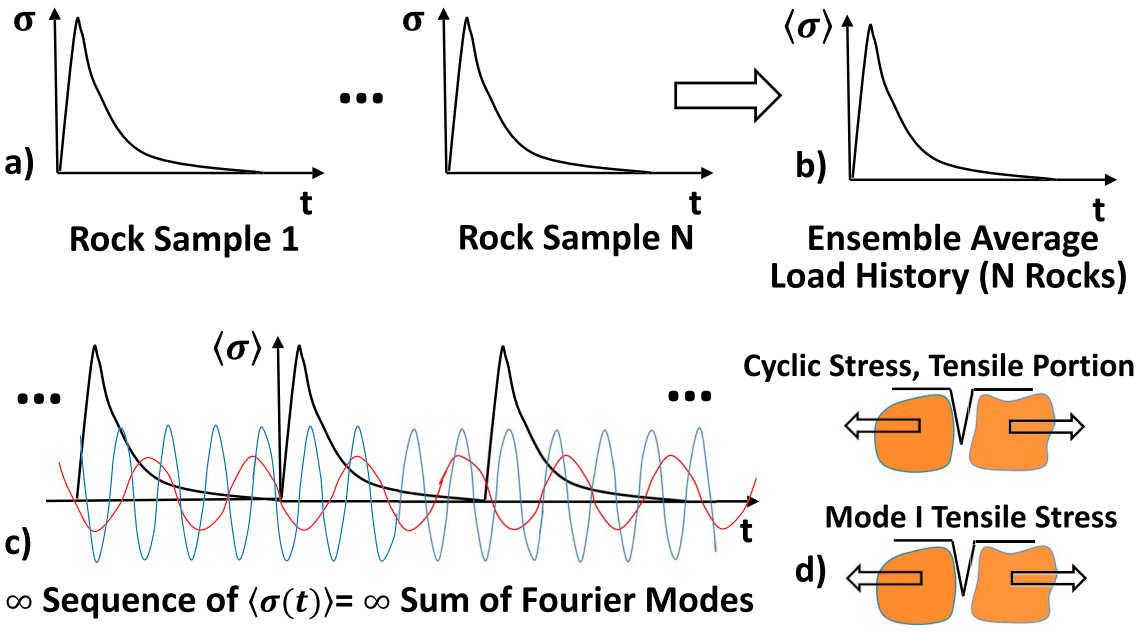

Figure A1. Pictorial representation of the argument leading to the equivalence, $m = n$, connecting the Paris law exponent, m, to the subcritical crack growth index, n. t = time; σ = tensile stress magnitude. (a) Imagine a large ensemble of N nominally identical rock samples, each subjected to the same Mode I initial ramp-up in tensile loading. (b) Due to random variations in grain-scale structure and mineralogy, individual stress relaxation responses—produced by subcritical cracking in each sample and depicted as the down turn in the curve—are likewise random. Since all N samples are nominally identical, however, a well-defined ensemble average stress relaxation, $\langle \sigma(t) \rangle -$, and associated ensemble average crack evolution, $\langle a(t) \rangle$, are realized. (c) If the hypothetical set of N subcritical fracture tests are repeated sequentially an infinite number of times, each individual set using a unique collection of N nominally identical rock samples, we would observe an infinite sequence of repeating ensemble average stress responses, $\langle \sigma(t) \rangle$, as shown. This cyclic sequence can then be mathematically recast as an infinite sum of individual Fourier modes. Physically, the latter can be interpreted as an infinite, linear, superposition of externally imposed subcritical cyclic loads. (d) Crucially, the ensemble average subcritical crack evolution, $\langle a(t) \rangle$, produced by either an infinite sequence of repeated Mode I tensile tests or by an infinite set of sequentially applied, purely sinusoidal subcritical cyclic fatigue loads is expected to be insensitive to the type of tensile loading—static versus cyclic—used. As detailed in the accompanying text, for grain-scale, near-surface, intergranular, subcritical cracking, any given grain-scale crack remains effectively "blind" to the mode by which external tensile stresses are imposed.

where δa_j and δa_k are combined and expressed as δa_β and where the Paris law correlation, equation (1) in the text, is assumed for each sinusoidal load component. In addition, the number of cycles,N_β, that the representative sample experiences under the β^{th} load, over the cycle period, $0 \le t < t_{\max}$, is given by $N_\beta = \beta$. Thus, discretize the total load interval, $[0, t_{\max})$, into $N_t$increments, $N_t \Delta t = t_{\max}$, and use [see, e.g., *Anderson*, 2005]

$$\left[\frac{\partial a}{\partial N}\right]_\beta = C_P \pi^{m/2} Y^m \, {\sigma_\beta}^m \, a^{m/2} \tag{A5}$$

in equation (A4) to finally obtain

$$\frac{da}{dt} = \left[C_P N_t \pi^{m/2-1} 2^{-1} Y^m \left[\sum_{\beta=1}^{\infty} \omega_\beta {\sigma_\beta}^m\right]\right] a^{m/2} \tag{A6}$$

where the frequency of the β^{th}sinusoidal load, ω_β, is related to β via $2\pi\beta = \omega_\beta N_t \Delta t$ and where $dt = \Delta t$ and $da = \delta a$.

Comparing the Charles law correlation in equation (A4) with the Paris law-based correlation in equation (A6), both of which describing the same crack evolution, we finally expose the following equalities tying the two correlations together:

$$m = n \tag{A7}$$

$$C_P N_t \pi^{m/2-1} 2^{-1} Y^m \left[\sum_{\beta=1}^{\infty} \omega_\beta {\sigma_\beta}^m\right] = C_c \pi^{n/2} Y^n \langle \sigma(t) \rangle^n \tag{A8}$$

Figure A1 schematically illustrates the preceding argument. Three points should be noted:

1. The ensemble average load history, $\langle \sigma(t) \rangle$, depicted in Figure A1b, can be viewed as representing the most probable stress-relaxation response to subcritical cracking that would, in principle, be observed in an actual rock test specimen. In this picture, the specimen is viewed as a sample taken from a hypothetical ensemble of *N* replica rocks, each undergoing the same initial Mode I loading. Due to random variations in grain-scale structure and mineralogy, individual responses exhibited by each rock in the ensemble exhibit random variations about $\langle \sigma(t) \rangle$.
2. Forming a repeating sequence of the ensemble load history, as depicted in Figure A1c, is mathematically allowed since $\langle \sigma(t) \rangle$ is a well-defined statistical function; physically, this procedure can be viewed as the average response that would be observed if an infinite set of *N*-rock ensembles were sequentially subjected to identical Mode I load tests.
3. Crucially, the essential equivalence of tensile static and cyclic load subcritical cracking, $m = n$, exposed by the above analysis, is expected to hold when the following assumptions and conditions are nominally met —under either static or cyclic loading: (a) subcritical cracking occurs near the rock surface and predominantly along grain boundaries; (b) grain-scale subcritical cracks are assumed to arrest predominantly at interleaving grains; (c) crack healing effects [e.g., *Anderson*, 2005]—due to low near-surface confining pressures—are assumed negligible; and (d) instantaneous near-crack stress fields—at any given Mode I tensile stress and at the same tensile stress under cyclic loading—are assumed to be identical (near any given crack in any given rock). Under these conditions, any near-surface, grain-scale crack remains "blind" to whether it is experiencing a single episode of Mode I tensile stress or the tensile phase of a cyclic load. Since, under these conditions, there are no stress history effects, the grain-scale crack responds (effectively) instantaneously—by incrementally growing the same small distance—regardless of the process by which the tensile stress is imposed (Figure A1d).

The correspondence in equation (A7), as already noted, is crucial to the development of predictive models of subcritical crack growth in rocks experiencing cyclic loading using existing empirical data. Specifically, this result allows substitution of existing empirical subcritical crack growth indices, *n*, with Paris law exponent, *m*. The former is obtained under laboratory conditions analytically through subcritical crack growth measurements under, e.g., constant stress or constant displacement conditions [e.g., *Atkinson and Meredith*, 1981; *Brantut et al.*, 2013].

Finally, we note that this appears to be the first time that the connection in equation (A7) has been made. Since the above argument is purely probabilistic, we believe that this equivalence holds for a wide range of granular materials subjected to steady, cyclic, or random (wholly or partly) tensile, subcritical loads.

Appendix B: Estimate of Critical Depth, z_{crit}, Below Which Weathering-Related Subcritical Cracking May Be Inhibited

Lithostatic stress, $\sigma_g = \sigma_g(z)$, increases approximately linearly with depth in rock:

$$\sigma_g(z) = \rho_{\text{rock}} g z + P_o \tag{B1}$$

where ρ_{rock} is the rock density (which will change with depth, although we do not consider that here), g is the gravitational acceleration, z is the depth below the subaerial surface, and P_o is ambient atmospheric pressure. A similar variation occurs when, for example, a rock layer is overlain by a layer of soil or regolith:

$$\sigma_g(z) = \rho_{\text{soil}} g h_{\text{soil}} + \rho_{\text{rock}} g z + P_o \tag{B2}$$

where h_{soil} is the soil depth and z is the depth below the soil-rock interface. In either case, and with increasing rock depth, compressive lithostatic stresses appear to increasingly suppress subcritical crack growth, a conclusion that is supported by both numerical modeling and experimental data [e.g., *Balme et al.*, 2004; *Rubin*, 1993; *Yao et al.*, 2016]. Here however, we seek to derive the maximum depth, z_{crit}, below which diurnally induced temperature cycling, and more generally, any environmentally induced tensile stresses, can no longer initiate subcritical crack growth.

In order to estimate z_{crit}, we express an approximate (order of magnitude) balance between the characteristic (absolute) depth-dependent diurnal temperature cycling-induced stress,

$$\sigma_{\text{diurnal}}(z) = \Delta\alpha E \Delta T_o \exp\left(-\sqrt{2\pi}\frac{z}{\delta_T}\right)/(1-\nu) + P_o \tag{B3}$$

and the characteristic depth-dependent lithostatic stress (equation (B2)), obtaining

$$\rho g z_{\text{crit}} \sim \Delta\alpha E \Delta T_o \exp\left(-\sqrt{2\pi}\frac{z_{\text{crit}}}{\delta_T}\right)/(1-\nu) \tag{B4}$$

Equation (B4) shows that the critical depth depends on a number of rock material properties, including Young's modulus, E; the characteristic difference between mineral thermal expansion coefficients, $\Delta\alpha$; bulk density, ρ; thermal diffusivity, κ (though the thermal penetration depth, $\delta_T = \sqrt{\kappa\Omega}$); and Poisson's ratio, ν, as well as a climate parameter, the characteristic (long timescale) diurnal (surface) temperature variation, ΔT_o.

This simple analysis shows that the ratio of characteristic thermal cycling-induced stress to confining pressure, $\sigma_{\text{diurnal}}(z)/\rho g z$, ranges from (effectively) infinity at the rock surface, $z = 0$, to magnitudes on the order of 1 to 10^2 at the thermal penetration depth, $z = \delta_T$. Thus, even at depths as large as δ_T, diurnal thermal stresses can still dominate the confining pressure; however, their efficacy is reduced. Experimental work examining these relationships is needed to validate this conclusion.

Appendix C: Calculations and Considerations for Intergranular Thermal Stresses

C1. Thermal Stress Response to Diurnal Heating

The time- and depth-dependent temperature field, $T = T(z, t)$, within a nominally planar rock, subject to sinusoidal surface heating and cooling, is obtained by a classic solution of the one-dimensional conductive heat transfer equation,

$$\frac{\partial T}{\partial t} = \kappa \frac{\partial^2 T}{\partial z^2} \tag{C1}$$

where $\kappa = k/\rho C_p$ is the bulk thermal diffusivity, k is the bulk thermal conductivity, ρ and C_p are the bulk density and specific heat, and the z axis is directed inward, perpendicular to the nominally planar surface. This form of the conduction equation assumes that the properties k, ρ, and C_p are isotropic and spatially uniform; in reality

most rocks, including granite, exhibit complex, nonisotropic thermophysical property variations [e.g., *Smith et al.*, 2011]. However, for relatively fine-grained rocks, not subject to temperature variations larger than approximately 100°C, and subject to small thermal stresses on the scales considered here, equation (C1) provides a reasonable description of thermal conduction.

For convenience, we restate the heat transfer problem in terms of the relative temperature, $\theta(z,t) = T(z,t) - T_\infty$, where T_∞ is the fixed far-field temperature at large depth, z, and the governing equation for $\theta(z,t)$ corresponds to equation (C1) with $T(z,t)$ replaced by $\theta(z,t)$. Following *Holzhausen* [1989], an idealized boundary condition is imposed at the rock surface, $z = 0$,

$$\theta(z=0,t) = T(z=0,t) - T_\infty = \Delta T_o \sin(\omega t) \tag{C2}$$

which is designed to capture diurnal temperature cycling. Here $\Delta T_o = T(z=0,t) - T_\infty$ is the magnitude of the diurnal surface temperature variation relative to T_∞, $\omega = \pi/\Omega$ and Ω is half the cycle's period (which we approximate as 12 h).

Given the boundary condition in equation (C2), equation (C3) yields the time- and depth-dependent temperature field:

$$T(z,t) - T_\infty = \Delta T_o \exp\left(-\sqrt{2\pi}\frac{z}{\delta_T}\right)\sin(\omega t - kz) \tag{C3}$$

where $\delta_T = \sqrt{\kappa\Omega}$ is the characteristic thermal penetration depth into the rock and $k = \frac{\sqrt{\frac{\pi}{2}}}{\delta_T}$.

Physically, equation (C3) shows that diurnal surface heating produces a plane wave, propagating vertically into the rock, with a wavelength, $\lambda = 2\pi/k = 2^{3/2}\pi^{1/2}\delta = \sqrt{8\pi}\delta_T$, and speed $c = \omega/k$. The amplitude of the inward-propagating wave, $\Delta T_o \exp\left[-\sqrt{\frac{\pi}{2}}\left(\frac{z}{\delta_T}\right)\right]$, decays exponentially with depth, decaying to evanescence on length scales on the order of the thermal penetration depth, δ_T. (Note that *Holzhausen* [1989] defines temperature variations relative to an assumed rock mean temperature; the appropriate reference temperature, in reality, is the far-field temperature, T_∞.)

As a point of reference, and due to the relatively high diffusivity of granite, our calculated δ_T, using parameters in Table 1, is on the order of 0.25 m. Because of light penetration and albedo effects, which can serve to further heat rock, this calculated depth likely represents a minimum but is nevertheless consistent with an earlier observation of δ_T (e.g., ~40 cm [*Anderson*, 1998]). By implication, thermal stresses and associated subcritical cracking, in any rock type, are essentially confined to the subsurface thermal penetration layer. The thermal penetration depth can vary significantly with topography [*Gischig et al.*, 2011a, 2011b], however, as well as both weather and annual climate.

Given the cyclically varying temperature field, $T(z,t)$, in equation (C3), and assuming thermally induced planar stress field yield [*Holzhausen*, 1989]

$$\sigma_{xx}(z,t) = \sigma_{yy}(z,t) = -\alpha E[T(z,t) - T_\infty]/(1-\nu) \tag{C4}$$

where E and ν are, respectively, Young's modulus and Poisson's ratio.

Briefly, equation (C4) follows by idealizing the planar rock as a semi-infinite, homogeneous, constant property region, whose planar, depth- and time-dependent stress response is governed by linear thermoelasticity. These are common idealizations in the fracture mechanics and thermoelastic material literature [e.g., *Anderson*, 2005; *Nowacki*, 2013]. Physically, equation (C4) shows that the elastic response tracks with the thermal response, so that exponentially damped planar thermal stress waves, having the same wavelength and speed as those associated with the temperature field, propagate into the rock.

C2. Calculating Intergranular Thermal Stress

C2.1. Theoretical and Practical Considerations

In order to develop a reasonable model of subcritical crack growth and associated cracking-driven rock erosion, the following must be well-identified: (i) a probable location of crack initiation, (ii) the essential physical mechanism(s) that transforms in-rock stresses into incipient cracks, and (iii) the *characteristic* minimum crack length, a_{min}, having non-negligible probability of subcritical growth.

Regarding probable locations of crack initiation, we assume that for low-magnitude stresses, such as the thermally induced stresses examined here, most cracks begin and propagate at, and along, grain boundaries (Figure 2 in the text)—or similarly, along grain-matrix boundaries in sedimentary rocks. This assumption is consistent with a finite element model [*Molaro and Byrne*, 2015], which showed that solar-induced microstructure-scale stresses peak at such boundaries. Preferential intergranular crack nucleation and propagation have also been demonstrated both experimentally and theoretically, regardless of the source of stress loading [e.g., *Butenuth*, 2001; *Johnson et al.*, 1978; *Potyondy*, 2007; *Sousa et al.*, 2005], and are generally recognized within the weathering community as a common mode of cracking, extant in a range of environments [e.g., *Ollier*, 1984; *Weiss et al.*, 2004].

In order to identify a physically reasonable, empirically supported mechanism through which stress is translated into cracking, and wishing to incorporate, in a simple manner, known properties of various granitic rocks, we introduce the following *ansatz*: granitic rock is idealized as being composed of two mineral constituents, quartz and feldspar. As noted in the text, a recent numerical model suggests that these minerals dominate the thermal stress and fracture response of granite [*Vázquez et al.*, 2015]. Thus, when computing the stress intensity amplitude, ΔK_I, in Paris's law, equation (1) in the text, we replace the bulk average thermal expansion coefficient, $-\alpha = \varphi\alpha_1 + \alpha_2,$ by the *difference* in thermal expansion coefficients for these two mineral constituents,

$$\Delta\alpha = \alpha_1 - \alpha_2 \tag{C5}$$

where φ is the volume fraction of mineral 1. This simple approach, which is explained physically in section C2.2 below, is also consistent with a complex, combined microscale and macroscale calculations of ΔK_I [*Delbo et al.*, 2014], as well as with a recent model of microstructure-scale thermal stresses [*Molaro and Byrne*, 2015]. As shown in our model validation (section 6 of the text), this approach leads to crack evolutions that over a range of characteristic surface temperature variations, ΔT, are quantitatively consistent with those predicted by a more complex, multiscale model [*Delbo et al.*, 2014].

Finally, and consistent with the assumption that cracks are predominantly initiated at intergranular boundaries, we assume that the minimum incipient crack length, $a_{\min}$, necessary for sustained, subsequent, subcritical crack growth is on the order of, but slightly smaller than, the characteristic grain size, $a_{\min} \equiv a_o \sim d_g$.

C2.2. Physical Justification

Unambiguous field evidence demonstrates the ubiquitous nature of presumably thermally driven granular disintegration in coarse grained rocks [e.g., *Eppes and Griffing*, 2010; *Gómez-Heras et al.*, 2006]. Thus, we briefly explore the physical aspects of this process as it relates to subcritical crack growth. Consider an idealized column of individual, contacting grains, where the column consists of a quasi-random arrangement of two constituent mineral grains. Any given grain remains in contact with the grain above and with the grain below. Assume, initially, that the column is isothermal but subsequently undergoes an overall temperature variation, from top to bottom, ΔT. For simplicity, assume that the Young's moduli for both grains are equal but that each grain has different thermal expansion coefficients, $\alpha_1$and α_2, respectively. In addition, for illustration, assume $\alpha_1 > \alpha_2$;the conclusions do not change if the opposite is true. Due to the mismatch in constituent α, and during positive temperature excursions, $\Delta T > 0$, both intergranular boundaries on any given grain experience a tensile stretching on the order of

$$\Delta x_1 - \Delta x_2 \sim (\alpha_1 \Delta T d_1 - \alpha_2 \Delta T d_2)/2 \tag{C6}$$

where the two terms on the right correspond to the thermally induced strains, $\epsilon_1$and ϵ_2, each multiplied by characteristic initial grain sizes, d_1, and d_2, respectively.

Considering first the case where d_1 and d_2 are of the same order of magnitude, $d_1 \sim d_2$, we divide both sides of equation (C6) by d_1 and compute the effective thermoelastic stress, $\Delta\sigma_{\text{eff}}$, produced at each intergranular boundary:

$$\Delta\sigma_{\text{eff}} \sim \Delta\alpha E \Delta T/(1-\nu) \quad \left(\text{for } d_1 \sim d_2\right) \tag{C7}$$

By contrast, under conditions where, e.g., $d_1 \gg d_2$,i.e., large grains are in contact with much smaller grains, intergranular contact is dominated by contact between grains having equal thermal expansion

coefficients, so that the first term on the right side of equation (C6) likewise dominates and the effective difference in thermal expansion coefficients, $\Delta\alpha \rightarrow \alpha_1$. In this case:

$$\Delta\sigma_{\text{eff}} \sim \alpha_1 E \Delta T/(1-\nu) \text{ (for } d_1 \gg d_2) \tag{C8}$$

Two central conclusions follow from equations (C7) and (C8):

1. In rocks where grain sizes are roughly of the same order of magnitude, i.e., $d_1 \sim d_2$, the appropriate stress for computing stress intensity is given approximately by equation (C7).
2. By contrast, in rocks like porphyries or poorly sorted sedimentary rocks, in which large grains are in contact with much smaller grains, i.e., $d_1 \gg d_2$, the appropriate intergranular stress is given approximately by equation (C8).

These conclusions are consistent with recent findings obtained via a complex finite element model of microstructure-scale thermal stresses produced by diurnal temperature cycling [*Molaro and Byrne*, 2015], as well as with recent experimental observations [*Vázquez et al.*, 2015].

Appendix D: Derivation and Validation of Approximate Paris Law Coefficient, *C*

Here we use a physically based, order of magnitude analysis to obtain an approximate expression for *C* as applicable to grainscale cracking that only incorporates known material properties and the Paris law exponent, *m*. In addition, in validating the proposed expression for *C*, we obtain further support for our physical picture of how cracking likely occurs in the near-surface region.

D1. Estimate

First, referring to equation (1) from the text, and focusing on the latter stages of crack evolution when increasing crack length causes the stress intensity factor, *K*, to approach the threshold, K_c,for critical crack growth, we approximate the associated crack extension per fatigue cycle, *da*/*dN*, as $a_c/1$:

$$da/dN \sim a_c/1 \tag{D1}$$

This approximation, which is also used by *Carpinteri and Paggi* [2007], applies as stress intensity approach K_c and assumes that prior to the approach toward critical cracking, crack growth is very slow. As $K \rightarrow K_c$, however, the change in crack length, Δa, over a small number, ΔN, of cycles is large and likely constitutes the majority of overall crack growth. This picture is supported theoretically by our calculations below, as well as by those reported by *Delbo et al.* [2014], both of which show long periods (on the order of 10^3 to 10^8 years) of extremely slow subcritical growth, followed by short periods of exponential crack growth. Experimentally, acoustic emission measurements of both freezing- and thermal-stress cracking, obtained for rock exposed under natural conditions, likewise show that measurable acoustic emission events exhibit short, intense, intermittent periods of activity (over intervals ranging from minutes to hours), corresponding to short, intermittent intervals of very high rates of cracking [*Eppes et al.*, 2016; *Girard et al.*, 2013; *Warren et al.*, 2013].

Crucially, at least with regard to estimating *C*, we hypothesize that in granular rocks, the *effective critical crack length*, $a_{c,\text{eff}}$, is only on the order d_g. We highlight this estimate as follows:

$$a_c \sim a_{c,\text{eff}} \sim d_g \tag{D2}$$

Given this estimate, we can now estimate *C* by first inserting the approximations in equations (D1) and (D2) into equation (1):

$$\frac{da}{dN} \sim \frac{d_g}{1} \sim C(\Delta K_I)^m$$

and then by approximating ΔK_I as the fracture toughness, K_c,

$$\frac{d_g}{1} \sim C K_c^m$$

finally yielding the approximation for C:

$$C \sim d_g K_c^{-m} \tag{D3}$$

D2. Validation

In order to test for reasonableness of the approximation in equation (D3), we use it to estimate *C*s for two materials having reported values of *C* that vary over 6 orders of magnitude: ordinary chondrites and 1020 hot rolled steel. If our estimate is generically applicable to most materials, it should match the reported values of *C* regardless of the magnitude. For ordinary chondrites, we assume that the fracture toughness is on the same order as that of Westerly granite, $K_{c\,,\,\mathrm{chondrite}} \sim K_{c\,,\,\mathrm{granite}} \approx 2$ MPa $\mathrm{m}^{1/2}$ and use $d_g = 2.3 \times 10^{-3}$ m and $m = 3.84$ [*Delbo et al.*, 2014] to obtain $C_{\mathrm{chondrite}} \sim 1.6 \times 10^{-4}$ m $[\mathrm{MPa}]^{-3.84}$. This value is comparable to $C_{\mathrm{chondrite}} \sim 3 \times 10^{-4}$ m $[\mathrm{MPa}]^{-3.84}$ given in *Delbo et al.* [2014]. Note too that the difference between the two values likely lies within the uncertainty bounds and property variability ranges associated with ordinary chondrite. For example, a 15% reduction in the assumed value of $K_{c\,,\,\mathrm{chondrite}}$ (to 1.7 MPa $\mathrm{m}^{1/2}$) leads to a predicted $C_{\mathrm{chondrite}}$ that matches that in *Delbo et al.* [2014]. As a second check, we use equation (D3) to estimate *C* for 1020 hot-rolled steel. Here using $K_{c,1020} \approx 80$ MPa $\mathrm{m}^{\frac{1}{2}}$ [*Klepaczko*, 1990], $d_g \approx 6 \times 10^{-5}$ m, and $m = 3.07$ [*Stephens et al.*, 1988, p 882] in equation (D3), we obtain $C_{1020} \sim 1.2 \times 10^{-10}$ m $[\mathrm{MPa}]^{-3.07}$. Even though this estimate is for a material whose *C* is reported as 6 orders of magnitude smaller than that for $C_{\mathrm{chondrite}}$, it is nevertheless comparable to the value of $C_{1020} = 2.96 \times 10^{-10}$ m $[\mathrm{MPa}]^{-3.07}$ for rolled steel measured in *Stephens et al.* [1988]. Again, by making moderate adjustments (~20%) to the assumed values of $K_{c\,,\,1020}$, d_g, and/or *m*—not unreasonable given material variability—an exact match with the measured C_{1020} can be obtained. Thus, lacking measured values for C for granite, we use the approximation in equation (D3). Moreover, since this relationship appears to hold for a range of materials, we surmise that it likely holds for other granular rock types.

Appendix E: Derivation and Validation of the Threshold Stress Intensity, K_{th}, Required for Subcritical Cracking

E1. Calculation

K_{th} represents the minimum stress intensity required for cracks to transition from nongrowing stasis to sustained subcritical growth. As previously mentioned in the text (section 2.2.8), this parameter has been generically reported in the literature as being 10%–20% of a material's fracture toughness,K_c; however, the time limitations of laboratory testing render these estimates as maximums since most experiments do not run sufficiently long to measure very slow crack growth [*Heap et al.*, 2009b]. In this appendix, we therefore focus on the physical and material parameters that likely determine the threshold stress intensity, K_{th}, in rock undergoing granular disintegration.

In order to estimate K_{th},

$$K_{\mathrm{th}} \sim \sigma_{\mathrm{min}} \sqrt{a_{\mathrm{min}}} \tag{E1}$$

physically reasonable assumptions regarding the characteristic minimum stress, σ_{min}, and the characteristic minimum crack length, a_{min}, must be introduced. Again, consistent with the assumption that cracks are predominantly initiated at intergranular boundaries, we assume that the minimum crack length, a_{min}, necessary for sustained subcritical crack growth is on the order of the characteristic grain size,

$$a_{\mathrm{min}} \sim d_g \tag{E2}$$

An estimate of σ_{min}, at least in an order of magnitude sense, is readily obtained by appealing to numerical, experimental, and field evidence showing that a wide variety of rock specimens exhibit observable intergranular cracking or fracture at tensile stresses on the order of the tensile strength, σ_T, or equivalently, the cohesive strength, $\sigma_{\mathrm{cohesive}}$ [*Butenuth*, 2001]. Thus,

$$\sigma_{\mathrm{min}} \cong \sigma_T \cong \sigma_{\mathrm{cohesive}} \tag{E3}$$

Using the estimates in equations (E2) and (E3) in (E1), we thus obtain a simple, material-dependent estimate for the threshold stress intensity:

$$K_{\mathrm{th}} \sim \sigma_T \sqrt{d_g} \tag{E4}$$

E2. Validation

In the case of granites, tensile strengths range from 5 to 20 MPa [*Afrouz*, 1992, p 39], while from, e.g., Table 1, $d_g \approx 7 \times 10^{-4}$ m. Thus, from equation (E4), we find that 0.1 MPa $m^{1/2} \lesssim K_{th\,,\,granite} \lesssim 0.5$ MPa $m^{1/2}$ consistent with *Atkinson*'s [1987] estimate for granite, $K_{th\,,\,granite} \sim 0.2$ MPa $m^{1/2}$.

As a second check on the estimate in equation (E4), (i) we define the characteristic, near-surface, diurnal temperature cycling-induced stress intensity as $K_{diurnal} = \frac{\Delta\alpha E \Delta T_o}{(1-\nu)}\sqrt{d_g}$, (ii) assume that significant near-surface subcritical cracking ensues when $K_{diurnal}$ approaches K_{th}, i.e., when $K_{diurnal} \sim K_{th}$, and (iii) solve for the corresponding threshold surface temperature variation, $\Delta T_{c\ granite}$, required for initiation of significant subcritical cracking in granite:

$$\Delta T_{c\ granite} \sim \sigma_T\ /\Delta\alpha E \tag{E5}$$

where the order unity $(1-\nu)$ term has been dropped. Using the above range of characteristic tensile strengths and the range of $\Delta\alpha$'s listed in Table 1, we find that the threshold diurnal temperature variation ranges roughly over $2\,^{\circ}C \lesssim \Delta T_{c\ granite} \lesssim 14\,^{\circ}C$,depending on the rock's combination of tensile strength and the mismatch between intergranular thermal expansion coefficients. No data exist that have tested such a threshold. Nevertheless, observations of cracking, as measured by acoustic emissions [*Eppes et al.*, 2016] in a natural granite boulder exposed to the Sun, suggest that while crack growth is not statistically correlated with diurnal temperature variations, measured crack growth rates accelerate appreciably at diurnal temperature ranges near ~20°C.

As a third, indirect check on the consistency of both the threshold stress intensity estimate in equation (E4) and the diurnal thermal stress-driven subcritical cracking model, we estimate the approximate ratio of the characteristic thermal cycling-related stress intensity to the characteristic fracture toughness,

$$K_{diurnal}/K_c \sim \frac{\Delta\alpha E \Delta T_o}{(1-\nu)}\sqrt{d_g}/K_c \tag{E6}$$

over a range of annual daily temperature variations, $15^{\circ} \le \Delta T_o \le 40^{\circ}C$, and the range of intergranular thermal expansion coefficient differences, $\Delta\alpha$, listed in Table 1. The estimate indicates that depending on climatic conditions—represented by ΔT_o—and rock material properties, this ratio ranges from $0.36 \lesssim K_{diurnal}/K_c \lesssim 1.79$.

Considered in light of the large body of experimental and field evidence demonstrating the ubiquity of temperature-related near surface cracking, these three observations have important implications:

1. Under a wide range of environmental conditions—as embodied by the characteristic diurnal rock surface temperature variation, ΔT_o—surface and near-surface diurnal thermal stresses are of sufficient magnitude to initiate subcritical cracking.
2. The assumption that the characteristic minimum crack length required for sustained subcritical growth is on the order of d_g appears reasonable.
3. Finally, and buttressed by the validation tests discussed in section 6 of the text, the above observations provide indirect support for our ansatz for estimating the effective diurnal cycling-induced stress, $\sigma_{diurnal} = \frac{\Delta\alpha E \Delta T_o}{(1-\nu)}$.

Appendix F: Estimating Random Variability in Rock and Environmental Parameters

F1. General Approach

This appendix outlines a method for estimating the *random relative variability*, $\delta r/r$, in any derived or modeled geological or geophysical quantity,

$$r = r(x_1, x_2, \ldots, x_N) \tag{F1}$$

which is produced by *random variabilities*, $\delta x_j/x_j$, in each of N random variables, $x_1, x_2, \ldots, x_N$, on which r depends. The function, $r = r(x_1, x_2, \ldots, x_N)$, representing either a closed form, analytical expression, or a numerical model, is either a *derived* expression, typically a parameterized experimental correlation involving the N variables, $x_1, x_2, \ldots, x_N$,whose detailed form is determined by fitting the expression to experimental

data, or a *modeled* expression, representing a model of some physical process, as obtained through a physical and mathematical analysis of the process.

The set of random variables, $x_1, x_2, \ldots, x_N$, include geologic parameters and properties that due to natural variations in, e.g., rock mineralogy, environmental exposure, and geologic history, vary in random ways and environmental variables that are likewise subject to random variability.

For example, and as discussed in section F3 below and in section 7.2.2, where we present a rough estimate of the random relative variability in estimated grain-scale, subcritical crack time, $\delta\tau_{c,\min}/\tau_{c,\min}$, r corresponds to $\tau_{c,\min}$, and the set of ($N = 3$)random variables that determine $\tau_{c,\min}$ is K_c, ΔK_I, and m.

F2. Derivation of Estimated Relative Variability, $\delta r/r$

In brief, we adapt a standard propagation of uncertainty argument [*Coleman and Steele*, 2009] to the task of estimating the random relative variability, $\delta r/r$, in the derived or modeled quantity, r. Crucially, extending the propagation of uncertainty argument to the estimation of the *random relative variability*, $\delta r/r$, is permissible since the broad, nonrestrictive statistical assumptions, and the mathematical steps [*Coleman and Steele*, 2009] used in the propagation of uncertainty argument—which leads to equation (F2) below—hold and can be applied here.

Thus, consider estimation of the *relative uncertainty*, $\delta f/f$, in a quantity, $f = f(y_1, y_2, \ldots, y_N)$, which depends on N *measured* (random) variables, $y_1, y_2, \ldots, y_N$, each of which is subject to a measured or estimated relative uncertainty, $\delta y_j/y_j$.Using a straightforward propagation of uncertainty argument [*Coleman and Steele*, 2009] leads to the following estimate for the relative uncertainty in r, produced by uncertainties in each of the random variables, y_j:

$$\left(\frac{\delta f}{f}\right) = \sqrt{\theta_1^2\left(\frac{\delta y_1}{y_1}\right)^2 + \theta_2^2\left(\frac{\delta y_2}{y_2}\right)^2 + \cdots + \theta_N^2\left(\frac{\delta y_N}{y_N}\right)^2} \tag{F2}$$

where

$$\theta_j^2 = \left(\frac{\partial f}{\partial y_j}\right)^2 \tag{F3}$$

As detailed, e.g., in *Coleman and Steele* [2009], equation (F2) is derived by Taylor expanding the function, $f = f(y_1, y_2, \ldots, y_N)$, about the true value of f, $f = f_{\text{true}} = f(y_{\text{true},1}, y_{\text{true},2}, \ldots, y_{\text{true},N})$, where, due to the fact that the true values of the random variables, $y_{\text{true},j}$, are unknown, f_{true} is likewise unknown. The principal mathematical assumption introduced in deriving equation (F2) is that second and higher order terms in the Taylor expansion of f about f_{true} are negligible relative to the first order terms, $\theta_j\delta y_j$, appearing in (F2). As discussed in section 7.2.2, in the case of estimates for $\delta\tau_{c,\min}/\tau_{c,\min}$, this assumption must be treated with caution.

In order to adapt the argument leading to the estimate for the *relative uncertainty*, $\delta f/f$, to estimating the *random relative variability*, $\delta r/r$, we only have to recognize that the same nonrestrictive statistical property assumed for the measured random variables, $y_1, y_2, \ldots, y_N$, generally holds for geophysical and climatic random variables, $x_1, x_2, \ldots, x_N$, namely, that the random probability distribution associated with each random variable, y_j or x_j, exists but is unspecified. (A further assumption underlies equation (F2): the function, $f = f(y_1, y_2, \ldots, y_N)$, or in the present case, $r = r(x_1, x_2, \ldots, x_N)$, is continuous and is continuously differentiable.)

Thus, we arrive at a generic expression that can be used to estimate the random relative variability, $\delta r/r$, produced by random variabilities, $\delta x_j/x_j$, in each of N random variables, $x_1, x_2, \ldots, x_N$, on which r depends

$$\left(\frac{\delta r}{r}\right) = \sqrt{\theta_1^2\left(\frac{\delta x_1}{x_1}\right)^2 + \theta_2^2\left(\frac{\delta x_2}{x_2}\right)^2 + \cdots + \theta_N^2\left(\frac{\delta x_N}{x_N}\right)^2} \tag{F4}$$

where

$$\theta_j^2 = \left(\frac{\partial r}{\partial x_j}\right)^2 \tag{F5}$$

F3. Application to Estimation of Random Relative Variability, $\delta\tau_{c,\min}/\tau_{c,\min}$, in Estimated Minimum Crack Lifetime, $\tau_{c,\min}$

Due to natural variability in the fracture mechanics properties, K_c, ΔK_I, and m, that determine the estimated minimum time, $\tau_{c,\min}$,

$$\tau_{c,\min} \sim [m(\langle \mathrm{RH} \rangle)/2 - 1]^{-1} [K_c/\Delta K_I]^{m(\langle \mathrm{RH} \rangle)} \tag{F6}$$

$\tau_{c,\min}$ is likewise subject to variability. Thus, (i) based on equation (F4); (ii) using equation (F6) to calculate the required partial derivatives, $\partial\tau_{c,\min}/\partial K_c = \theta_1$, $\partial\tau_{c,\min}/\partial(\Delta K_I) = \theta_2$, and $\partial\tau_{c,\min}/\partial m = \theta_3$, as represented by equation (F5); and (iii) following straightforward manipulation, we obtain

$$\left(\frac{\delta\tau_{c,\min}}{\tau_{c,\min}}\right) = \sqrt{m^2\left(\frac{\delta K_c}{K_c}\right)^2 + m^2\left(\frac{\delta(\Delta K_I)}{(\Delta K_I)}\right)^2 + \left[\ln(\tau_{c,\min}) - m^{-1}\right]^2\left(\frac{\delta m}{m}\right)^2} \tag{F7}$$

Further details on the application of equation (F7) to the estimation of $\delta\tau_{c,\min}/\tau_{c,\min}$ are described in section 7.2.2.

F4. Calculations for Figure 4b

Estimation of mean ΔK_I and of the relative variability, $\delta(\Delta K_I)/\Delta K_I$, depends on the model or models used to estimate environmental crack-tip stress intensity variations, ΔK_I. We do not consider those in detail here. Nevertheless, we note that for strictly solar-driven subcritical cracking, equations (2) and (3) in the text lead to the following theoretical expression for ΔK_I: $\Delta K_I = \Delta K_I(\Delta\alpha, E, \nu, \Delta T_o, a) = \Delta\alpha E \Delta T_o \sqrt{\pi a}/(1-\nu)$. In order to derive an expression giving an estimate for $\delta(\Delta K_I)/\Delta K_I$, the same mathematical procedure outlined herein could be applied to the function $\Delta K_I = \Delta K_I(\Delta\alpha, E, \nu, \Delta T_o, a)$. Similarly, the same mathematical procedure could likewise be used for any climate- or environment-based model used to derive a theoretical expression for ΔK_I.

Unfortunately, at present, available data for most rocks including granite are not sufficient to allow reliable estimates of means and variabilities for many primary material properties. Thus, in order to obtain a rough but reasonable estimate of the band of variability, $\delta\tau_{c,\min}$, expected in estimated minimum subcritical crack lifetimes depicted in Figure 4, we assume that $\delta K_c/K_c \sim 0.5$ (based on the range of values presented in *Atkinson* [1987]) and that $\delta(\Delta K_I)/\Delta K_I \sim 0.5$. In addition, and focusing on Westerly granite where observed stress corrosion indices, $n = m$, are in the approximate range $\sim 40 < m < \sim 85$ [*Atkinson*, 1987; *Nara et al.*, 2013], equation (F7) can be simplified by assuming that the relative variabilities, $\delta K_c/K_c$, $\delta(\Delta K_I)/\Delta K_I$, and $\delta m/m$ are all roughly of the same order of magnitude and by noting that $m^2 \gg [\ln(\tau_{c,\min}) - m^{-1}]^2$. Under these circumstances, the third term on the right side of (F7) can be neglected. Finally, as an estimate for the mean, humidity-dependent Paris law exponent, m, we again use *Nara et al.* [2013] to express m as $m = m_o - m_1 \times \langle \mathrm{RH} \rangle$, where again, $m_o = 80.4$ and $m_1 = 0.28$.

Appendix G: Approximation for the Climatology of Diurnal Temperature Ranges

We use a simple probabilistic model of random daily temperature variations, ΔT, to estimate the number of days, $n_{\Delta T}$, during any given year that $|\Delta T|$ exceeds $|\Delta T_c|$. Here consistent with the sigmoidal dependence of $\tau_{c,\min}$ on ΔT, which arises due to exponentiation of ΔT by the stress corrosion index, $m = n$—see equations (9) and (10) in the text—we assume the existence of a critical temperature variation, ΔT_c; specifically, the model assumes that significant subcritical cracking only occurs when the daily ΔT approaches, and either exceeds ΔT_c (warm climates) or, in cold climates, drops below $-\Delta T_c$. We found only a single data set that included a long-term rock surface temperature range distribution [*Eppes et al.*, 2015a]. Temperatures therein were roughly normally distributed. Thus, given the overall lack of such data, assuming a Gaussian distribution for daily ΔT's is a reasonable first approximation and, more importantly, circumvents the unrealistic assumption that ΔT remains, on all days, uniform and equal to an annual average.

For simplicity, and for any given location, assume that the random daily maximum temperature variation, ΔT, is Gaussian:

$$p(\Delta T) = \frac{1}{\sqrt{2\,\pi\sigma_{\Delta T}^2}} \exp\left[\frac{-(\Delta T - < \Delta T >)^2}{2\sigma_{\Delta T}^2}\right] \tag{G1}$$

where $p(\Delta T)$ is the probability density; $\langle \Delta T \rangle$ is the mean daily variation over some time period, for example, a year; and $\sigma^2_{\Delta T} = \left\langle \left(\Delta T - \langle \Delta T \rangle \right)^2 \right\rangle$ is the associated variance.

In general, given an assumed or known $p(\Delta T)$,not necessarily Gaussian, the number of days per year, $n_{\Delta T}$, that ΔT exceeds ΔT_c is given by

$$n_{\Delta T} = N_o \left[\int_{\Delta T'_c}^{\infty} p\left(\Delta T'\right) d\Delta T' + \int_{-\infty}^{-\Delta T'_c} p\left(\Delta T'\right) d\Delta T' \right] \tag{G2}$$

where $\Delta T' = \Delta T - \langle \Delta T \rangle$ is the daily variation relative to the mean, $\Delta T'_c = \Delta T_c - \langle \Delta T \rangle$, and N_o is the number of days per year ($N_o = 365$). The first and second terms on the right side of equation (G2) (i) account, respectively, for cracking events that occur on warm and cold days and (ii) represent, respectively, the (cumulative) probability of observing, on any given day, positive temperature variations, ΔT, exceeding ΔT_c, or negative variations, $-\Delta T$, having magnitudes, $|\Delta T|$, again exceeding ΔT_c.

In regions where a Gaussian density represents a reasonable model for ΔT, i.e., regions with moderately warm summers and moderately cold winters, equation (G2) can be integrated to obtain a closed form relationship for the frequency per year, $f_{\text{solar}} = n_{\Delta T} N_o^{-1}$, that daily temperature variations exceed ΔT_c:

$$f_{\text{solar}} = f_{\text{solar}}(\Delta T_c) = \frac{n_{\Delta T}}{N_o} = 1 + \frac{1}{2} \operatorname{erf}\left[\frac{-\Delta T'_c}{2\sigma_{\Delta T}}\right] - \frac{1}{2} \operatorname{erf}\left[\frac{\Delta T'_c}{2\sigma_{\Delta T}}\right] \tag{G3}$$

where erf(x) is the error function. The fraction,$f_{\text{solar}}(\Delta T_c)$, is used in our model of thermal cycling-driven, moisture-dependent rock erosion.

Acknowledgments

The authors would like to acknowledge the inspiration, encouragement, and feedback for this work received during conversations with Bernard Hallet, Amit Mushkin, David Harbor, John Diemer, Les McFadden, and Chris Conners. Eppes would also like to thank the students, colleagues, and friends who continue to act as perpetual sounding boards for these ideas that fall on the fringes of conventional soils and geomorphology research. This research did not receive any specific grant from funding agencies in the public, commercial, or not-for-profit sectors. The data used are listed in the references cited and the tables presented.

References

Adelsberger, K. A., and J. R. Smith (2009), Desert pavement development and landscape stability on the Eastern Libyan Plateau, Egypt, *Geomorphology*, *107*(3), 178–194.

Afrouz, A. (1992), *Practical Handbook of Rock Mass Classification Systems and Modes of Ground Failure*, CRC Press, Boca Raton, Fla.

Al-Omari, A., X. Brunetaud, K. Beck, and M. Al-Mukhtar (2014), Effect of thermal stress, condensation and freezing–thawing action on the degradation of stones on the Castle of Chambord, France, *Environ. Earth Sci.*, *71*(9), 3977–3989.

Aldred, J., M. C. Eppes, K. Aquino, R. Deal, J. Garbini, S. Swami, A. Tuttle, and G. Xanthos (2015), The influence of solar-induced thermal stresses on the mechanical weathering of rocks in humid mid-latitudes, *Earth Surf. Processes Landforms*, *41*, 603–614.

Amaral, P. M., L. Guerra Rosa, and J. Cruz Fernandes (2008), Assessment of fracture toughness in ornamental stones, *Int. J. Rock Mech. Min. Sci.*, *45*(4), 554–563.

Amit, R., R. Gerson, and D. Yaalon (1993), Stages and rate of the gravel shattering process by salts in desert Reg soils, *Geoderma*, *57*(3), 295–324.

Amitrano, D., and A. Helmstetter (2006), Brittle creep, damage, and time to failure in rocks, *J. Geophys. Res.*, *111*, B11201, doi:10.1029/2005JB004252.

Anderson, O. L., and P. C. Grew (1977), Stress corrosion theory of crack propagation with applications to geophysics, *Rev. Geophys.*, *15*(1), 77–104.

Anderson, R. S. (1998), Near-surface thermal profiles in alpine bedrock: Implications for the frost weathering of rock, *Arct. Alp. Res.*, *30*, 362–372.

Anderson, T. L. (2005), *Fracture Mechanics: Fundamentals and Applications*, CRC Press, Boca Raton, Fla.

Atkinson, B. K. (1979), A fracture mechanics study of subcritical tensile cracking of quartz in wet environments, *Pure Appl. Geophys.*, *117*(5), 1011–1024.

Atkinson, B. K. (1984), Subcritical crack growth in geological materials, *J. Geophys. Res.*, *89*(B6), 4077–4114.

Atkinson, B. K. (1987), *Fracture Mechanics of Rock*, Academic Press, London.

Atkinson, B. K., and P. G. Meredith (1981), Stress corrosion cracking of quartz: A note on the influence of chemical environment, *Tectonophysics*, *77*(1), T1–T11.

Atkinson, B. K., and P. G. Meredith (1987), The theory of subcritical crack growth with applications to minerals and rocks, in *Fracture Mechanics of Rock*, edited by B. K. Atkinson, pp. 111–166, Academic Press, London.

Attewell, P., and I. Farmer (1973), Fatigue behaviour of rock, paper presented at International Journal of Rock Mechanics and Mining Sciences & Geomechanics Abstracts, Elsevier.

Balme, M., V. Rocchi, C. Jones, P. Sammonds, P. Meredith, and S. Boon (2004), Fracture toughness measurements on igneous rocks using a high-pressure, high-temperature rock fracture mechanics cell, *J. Volcanol. Geotherm. Res.*, *132*(2), 159–172.

Barnett, R., and R. Kerrich (1980), Stress corrosion cracking of biotite and feldspar, *Nature*, *283*, 185–187.

Batjes, N. (1995), *A Global Data Set of Soil pH Properties Rep*, International Soil Reference and Information Center (ISRIS), Wageningen, Netherlands.

Bazilevskaya, E., M. Lebedeva, M. Pavich, G. Rother, D. Y. Parkinson, D. Cole, and S. L. Brantley (2013), Where fast weathering creates thin regolith and slow weathering creates thick regolith, *Earth Surf. Processes Landforms*, *38*(8), 847–858.

Birkeland, P. W. (1982), Subdivision of Holocene glacial deposits, Ben Ohau Range, New Zealand, using relative-dating methods, *Geol. Soc. Am. Bull.*, *93*(5), 433–449.

Bost, M., and A. Pouya (2016), Stress generated by the freeze-thaw process in open cracks of rock walls: Empirical model for tight limestone, *Bull. Eng. Geol. Environ.*, *1-15*.

Brain, M. J., N. J. Rosser, E. C. Norman, and D. N. Petley (2014), Are microseismic ground displacements a significant geomorphic agent?, *Geomorphology*, *207*, 161–173.
Brantut, N., M. Heap, P. Meredith, and P. Baud (2013), Time-dependent cracking and brittle creep in crustal rocks: A review, *J. Struct. Geol.*, *52*, 17–43.
Brantut, N., M. J. Heap, P. Baud, and P. G. Meredith (2014a), Mechanisms of time-dependent deformation in porous limestone, *J. Geophys. Res. Solid Earth*, *119*, 5444–5463, doi:10.1002/2014JB011186.
Brantut, N., M. Heap, P. Baud, and P. Meredith (2014b), Rate-and strain-dependent brittle deformation of rocks, *J. Geophys. Res. Solid Earth*, *119*, 1818–1836, doi:10.1002/2013JB010448.
Burke, B. C., A. M. Heimsath, and A. F. White (2007), Coupling chemical weathering with soil production across soil-mantled landscapes, *Earth Surf. Processes Landforms*, *32*(6), 853–873.
Burke, R., and P. W. Birkeland (1979), Reevaluation of multiparameter relative dating techniques and their application to the glacial sequence along the eastern escarpment of the Sierra Nevada, California, *Quatern. Res.*, *11*(1), 21–51.
Burnett, B. N., G. A. Meyer, and L. D. McFadden (2008), Aspect-related microclimatic influences on slope forms and processes, northeastern Arizona, *J. Geophys. Res.*, *113*, F03002, doi:10.1029/2007JF000789.
Butenuth, C. (2001), *Strength and Weathering of Rock as Boundary Layer Problems*, Imperial College Pres, London, U. K.
Carpinteri, A., and M. Paggi (2007), Are the Paris' law parameters dependent on each other?, *Fracture and Structural Integrity*, *2*, 10–16.
Chan, W.-P., I.-C. Chen, R. K. Colwell, W.-C. Liu, C.-y. Huang, and S.-F. Shen (2016), Seasonal and daily climate variation have opposite effects on species elevational range size, *Science*, *351*(6280), 1437–1439.
Charles, R. (1958), Static fatigue of glass. I, *J. Appl. Phys.*, *29*(11), 1549–1553.
Chau, K., and J.-F. Shao (2006), Subcritical crack growth of edge and center cracks in façade rock panels subject to periodic surface temperature variations, *Int. J. Solids Struct.*, *43*(3), 807–827.
Christensen, N., and H. Wang (1985), The influence of pore pressure and confining pressure on dynamic elastic properties of Berea sandstone, *Geophysics*, *50*(2), 207–213.
Coleman, H. W., and W. G. Steele (2009), Experimentation, validation, and uncertainty analysis for engineers, John Wiley, Hoboken, N. J.
Collins, B. D., and G. M. Stock (2016), Rockfall triggering by cyclic thermal stressing of exfoliation fractures, *Nat. Geosci.*, *9*, 395–400.
Costin, L. (1985), Damage mechanics in the post-failure regime, *Mech. Mater.*, *4*(2), 149–160.
Costin, L., and D. Holcomb (1981), Time-dependent failure of rock under cyclic loading, *Tectonophysics*, *79*(3), 279–296.
Dai, A. (2006), Recent climatology, variability, and trends in global surface humidity, *J. Clim.*, *19*(15), 3589–3606.
Dai, F., and K. Xia (2010), Loading rate dependence of tensile strength anisotropy of Barre granite, *Pure Appl. Geophys.*, *167*(11), 1419–1432.
Delbo, M., G. Libourel, J. Wilkerson, N. Murdoch, P. Michel, K. Ramesh, C. Ganino, C. Verati, and S. Marchi (2014), Thermal fatigue as the origin of regolith on small asteroids, *Nature*, *508*(7495), 233–236.
Dove, P. M. (1995), Geochemical controls on the kinetics of quartz fracture at subcritical tensile stresses, *J. Geophys. Res.*, *100*(B11), 22,349–22,359.
Draebing, D., M. Krautblatter, and T. Hoffman (2017), Thermo-cryogenic controls of fracture kinematics in permafrost rockwalls, *Geophys. Res. Lett.*, *4*(8), 3535–3544, doi:10.1002/2016GL072050.
Dunning, J., B. Douglas, M. Miller, and S. McDonald (1994), The role of the chemical environment in frictional deformation: Stress corrosion cracking and comminution, *Pure Appl. Geophys.*, *143*(1–3), 151–178.
Eberhardt, E., D. Stead, B. Stimpson, and R. Read (1998), Identifying crack initiation and propagation thresholds in brittle rock, *Can. Geotech. J.*, *35*(2), 222–233.
Elliott, C. (2004), Surface moisture availability and rock weathering in cold climates, *N. Z. Geogr.*, *60*(1), 44–51.
Elliott, C. (2008), Influence of temperature and moisture availability on physical rock weathering along the Victoria land coast, Antarctica, *Antarct. Sci.*, *20*(01), 61–67.
Eppes, B., B. Magi, E. Hallet, P. Delmelle, K. W. Mackenzie-Helnwein, and S. Swami (2016), Deciphering the role of solar-induced thermal stresses in rock weathering, *Geol. Soc. Am. Bull.*, *128*(9–10), 1315–1338.
Eppes, M. C., and D. Griffing (2010), Granular disintegration of marble in nature: A thermal-mechanical origin for a grus and corestone landscape, *Geomorphology*, *117*(1), 170–180.
Eppes, M. C., K. Warren, E. Hinson, and L. Dash (2012), Long term monitoring of rock surface temperature and rock cracking in temperate and desert climates, Abstract EP41F-0848 presented at 2012 Fall Meeting, AGU, San Francisco, Calif.
Eppes, M. C., B. Magi, and R. Keanini (2015a), Real-time observations of rock cracking and weather provide insights into thermal stress-related processes of mechanical weathering, Abstract EP41C-0942 presented at 20115 Fall Meeting, AGU, San Francisco, Calif., 14–18 Dec.
Eppes, M. C., A. Willis, J. Molaro, S. Abernathy, and B. Zhou (2015b), Cracks in Martian boulders exhibit preferred orientations that point to solar-induced thermal stress, *Nat. Commun.*, *6*, 6712.
Fei, Y. (1995), Thermal expansion, in *Mineral Physics and Crystallography: A Handbook of Physical Constants*, vol. 2, pp. 29–44, AGU, Washington, D. C.
Fletcher, R., and S. Brantley (2010), Reduction of bedrock blocks as corestones in the weathering profile: Observations and model, *Am. J. Sci.*, *310*(3), 131–164.
Freire-Lista, D. M., R. Fort, and M. J. Varas-Muriel (2016), Thermal stress-induced microcracking in building granite, *Eng. Geol.*, *206*, 83–93.
Garcin, Y., T. F. Schildgen, V. T. Acosta, D. Melnick, J. Guillemoteau, J. Willenbring, and M. R. Strecker (2017), Short-lived increase in erosion during the African Humid Period: Evidence from the northern Kenya Rift, *Earth Planet. Sci. Lett.*, *459*, 58–69.
Gerber, E., and A. Scheidegger (1969), Stress-induced weathering of rock masses, *Eclogae Geol. Helv.*, *62*(2), 401–415.
Gercek, H. (2007), Poisson's ratio values for rocks, *Int. J. Rock Mech. Min. Sci.*, *44*(1), 1–13.
Girard, L., S. Gruber, S. Weber, and J. Beutel (2013), Environmental controls of frost cracking revealed through in situ acoustic emission measurements in steep bedrock, *Geophys. Res. Lett.*, *40*, 1748–1753, doi:10.1002/grl.50384.
Gischig, V. S., J. R. Moore, K. F. Evans, F. Amann, and S. Loew (2011a), Thermomechanical forcing of deep rock slope deformation: 1. Conceptual study of a simplified slope, *J. Geophys. Res.*, *116*, F04010, doi:10.1029/2011JF002006.
Gischig, V. S., J. R. Moore, K. F. Evans, F. Amann, and S. Loew (2011b), Thermomechanical forcing of deep rock slope deformation: 2. The Randa rock slope instability, *J. Geophys. Res.*, *116*, F04011, doi:10.1029/2011JF002007.
Gómez-Heras, M., B. J. Smith, and R. Fort (2006), Surface temperature differences between minerals in crystalline rocks: Implications for granular disaggregation of granites through thermal fatigue, *Geomorphology*, *78*(3), 236–249.
Goudie, A. S. (2013), *Arid and Semi-Arid Geomorphology*, Cambridge Univ. Press, Cambridge, U. K.
Grgic, D., and D. Amitrano (2009), Creep of a porous rock and associated acoustic emission under different hydrous conditions, *J. Geophys. Res.*, *114*, B10201, doi:10.1029/2006JB004881.

Griffiths, L., M. J. Heap, T. Xu, C.-f. Chen, and P. Baud (2017), The influence of pore geometry and orientation on the strength and stiffness of porous rock, *J. Struct. Geol.*, *96*, 149–160.
Griggs, D. T. (1936), The factor of fatigue in rock exfoliation, *J. Geol.*, *44*, 783–796.
Gupta, A., and K. S. Rao (2000), Weathering effects on the strength and deformational behaviour of crystalline rocks under uniaxial compression state, *Eng. Geol.*, *56*(3), 257–274.
Haas, T., S. J. Conway, and M. Krautblatter (2015), Recent (Late Amazonian) enhanced backweathering rates on Mars: Paracratering evidence from gully alcoves, *J. Geophys. Res. Planets*, *120*, 2169–2189, doi:10.1002/2015JE004915.
Hadizadeh, J., and R. Law (1991), Water-weakening of sandstone and quartzite deformed at various stress and strain rates, paper presented at International journal of rock mechanics and mining sciences & geomechanics abstracts, Pergamon.
Hales, T., and J. J. Roering (2007), Climatic controls on frost cracking and implications for the evolution of bedrock landscapes, *J. Geophys. Res.*, F02033, *112*, doi:10.1029/2006JF000616.
Hall, K. (1986), Rock moisture content in the field and the laboratory and its relationship to mechanical weathering studies, *Earth Surf. Processes Landforms*, *11*(2), 131–142.
Hall, K., and M.-F. André (2001), New insights into rock weathering from high-frequency rock temperature data: An Antarctic study of weathering by thermal stress, *Geomorphology*, *41*(1), 23–35.
Hall, K., and A. Hall (1996), Weathering by wetting and drying: Some experimental results, *Earth Surf. Processes Landforms*, *21*(4), 365–376.
Hall, K., and C. E. Thorn (2014), Thermal fatigue and thermal shock in bedrock: An attempt to unravel the geomorphic processes and products, *Geomorphology*, *206*, 1–13.
Hall, K., B. S. Lindgren, and P. Jackson (2005), Rock albedo and monitoring of thermal conditions in respect of weathering: Some expected and some unexpected results, *Earth Surf. Processes Landforms*, *30*(7), 801–811.
Hall, K., I. Meiklejohn, P. Sumner, and J. Arocena (2010), Light penetration into Clarens sandstone and implications for deterioration of San rock art, *Geoarchaeology*, *25*(1), 122–136.
Halsey, D., D. Mitchell, and S. Dews (1998), Influence of climatically induced cycles in physical weathering, *Q. J. Eng. Geol. Hydrogeol.*, *31*(4), 359–367.
Harris, I., P. Jones, T. Osborn, and D. Lister (2014), Updated high-resolution grids of monthly climatic observations—The CRU TS3. 10 dataset, *Int. J. Climatol.*, *34*(3), 623–642.
Heap, M., and D. Faulkner (2008), Quantifying the evolution of static elastic properties as crystalline rock approaches failure, *Int. J. Rock Mech. Min. Sci.*, *45*(4), 564–573.
Heap, M., P. Baud, and P. Meredith (2009a), Influence of temperature on brittle creep in sandstones, *Geophys. Res. Lett.*, L19305, *36*, doi:10.1029/2009GL039373.
Heap, M., P. Baud, P. Meredith, A. Bell, and I. Main (2009b), Time-dependent brittle creep in Darley Dale sandstone, *J. Geophys. Res.*, *114*, B07203, doi:10.1029/2008JB006212.
Heap, M., P. Baud, P. Meredith, S. Vinciguerra, A. Bell, and I. Main (2011), Brittle creep in basalt and its application to time-dependent volcano deformation, *Earth Planet. Sci. Lett.*, *307*(1), 71–82.
Heap, M. J., T. Xu, and C.-f. Chen (2014), The influence of porosity and vesicle size on the brittle strength of volcanic rocks and magma, *Bull. Volcanol.*, *76*(9), 1–15.
Heimsath, A. M., W. E. Dietrich, K. Nishiizumi, and R. C. Finkel (1997), The soil production function and landscape equilibrium, *Nature*, *388*(6640), 358–361.
Heimsath, A. M., R. A. DiBiase, and K. X. Whipple (2012), Soil production limits and the transition to bedrock-dominated landscapes, *Nat. Geosci.*, *5*(3), 210–214.
Hoke, G. D., and D. L. Turcotte (2002), Weathering and damage, *J. Geophys. Res.*, *107*(B10), 2210, doi:10.1029/2001JB001573.
Holder, J., J. E. Olson, and Z. Philip (2001), Experimental determination of subcritical crack growth parameters in sedimentary rock, *Geophys. Res. Lett.*, *28*(4), 599–602.
Holzhausen, G. R. (1989), Origin of sheet structure. Morphology and boundary conditions 1, *Eng. Geol.*, *27*(1), 225–278.
Hooke, R. L. (1991), Positive feedbacks associated with erosion of glacial cirques and overdeepenings, *Geol. Soc. Am. Bull.*, *103*(8), 1104–1108.
Humphreys, G. S., and M. T. Wilkinson (2007), The soil production function: A brief history and its rediscovery, *Geoderma*, *139*(1), 73–78.
Ishikawa, M., Y. Kurashige, and K. Hirakawa (2004), Analysis of crack movements observed in an alpine bedrock cliff, *Earth Surf. Processes Landforms*, *29*(7), 883–891.
Jeong, H.-S., S.-S. Kang, and Y. Obara (2007), Influence of surrounding environments and strain rates on the strength of rocks subjected to uniaxial compression, *Int. J. Rock Mech. Min. Sci.*, *44*(3), 321–331.
Jia, H., W. Xiang, and M. Krautblatter (2015), Quantifying rock fatigue and decreasing compressive and tensile strength after repeated freeze-thaw cycles, *Permafr. Periglac. Proc.*, *26*(4), 368–377.
Jiménez-González, I., C. Rodríguez-Navarro, and G. W. Scherer (2008), Role of clay minerals in the physicomechanical deterioration of sandstone, *J. Geophys. Res.*, *113*, F02021, doi:10.1029/2007JF000845.
Johnson, B., A. Gangi, and J. Handin (1978), Thermal cracking of rock subjected to slow uniform temperature changes, paper presented at 19th U.S. Symposium on Rock Mechanics (USRMS), American Rock Mechanics Association.
Jones, R. H. (1992), *Stress-Corrosion Cracking*, ASM International, Materials Park, OH.
Kirchner, J. W., C. S. Riebe, K. L. Ferrier, and R. C. Finkel (2006), Cosmogenic nuclide methods for measuring long-term rates of physical erosion and chemical weathering, *J. Geochem. Explor.*, *88*(1), 296–299.
Klepaczko, J. (1990), Dynamic crack initiation, some experimental methods and modelling, in *Crack Dynamics in Metallic Materials*, pp. 2555–2453, Springer, New York.
Knight, J., and S. W. Grab (2014), Lightning as a geomorphic agent on mountain summits: Evidence from southern Africa, *Geomorphology*, *204*, 61–70.
Kranz, R. L. (1979), Crack growth and development during creep of Barre granite, paper presented at International Journal of Rock Mechanics and Mining Sciences & Geomechanics Abstracts, Elsevier.
Kranz, R. L., W. J. Harris, and N. L. Carter (1982), Static fatigue of granite at 200°C, *Geophys. Res. Lett.*, *9*(1), 1–4.
Kudo, Y., O. Sano, N. Murashige, Y. Mizuta, and K. Nakagawa (1992), Stress-induced crack path in Aji granite under tensile stress, *Pure Appl. Geophys.*, *138*(4), 641–656.
Lamp, J., D. Marchant, S. Mackay, and J. Head (2017), Thermal stress weathering and the spalling of Antarctic rocks, *J. Geophys. Res. Earth Surf.*, *122*, 3–24, doi:10.1002/2016JF003992.
Langston, A. L., G. E. Tucker, R. S. Anderson, and S. P. Anderson (2015), Evidence for climatic and hillslope-aspect controls on vadose zone hydrology and implications for saprolite weathering, *Earth Surf. Processes Landforms*, *40*(9), 1254–1269.

Larsen, I. J., P. C. Almond, A. Eger, J. O. Stone, D. R. Montgomery, and B. Malcolm (2014), Rapid soil production and weathering in the Southern Alps, New Zealand, *Science*, *343*(6171), 637–640.
Lawn, B. (1993), *Fracture of Brittle Solids*, Cambridge Univ. Press, Cambridge, U. K.
Lebedeva, M. I., and S. L. Brantley (2017), Weathering and erosion of fractured bedrock systems, *Earth Surf. Processes Landforms*, doi:10.1002/esp.4177.
Leith, K., J. R. Moore, F. Amann, and S. Loew (2014), In situ stress control on microcrack generation and macroscopic extensional fracture in exhuming bedrock, *J. Geophys. Res. Solid Earth*, *119*, 594–615, doi:10.1002/2012JB009801.
Levenson, Y., U. Ryb, and S. Emmanuel (2017), Comparison of field and laboratory weathering rates in carbonate rocks from an eastern Mediterranean drainage basin, *Earth Planet. Sci. Lett.*, *465*, 176–183.
Lockner, D. (1993), The role of acoustic emission in the study of rock fracture, paper presented at International Journal of Rock Mechanics and Mining Sciences & Geomechanics Abstracts, Elsevier.
Martel, S. J. (2006), Effect of topographic curvature on near-surface stresses and application to sheeting joints, *Geophys. Res. Lett.*, *33*, L01308, doi:10.1029/2005GL024710.
Martel, S. J. (2011), Mechanics of curved surfaces, with application to surface-parallel cracks, *Geophys. Res. Lett.*, *38*, L20303, doi:10.1029/2011GL049354.
Matsukura, Y., and K. I. Takahashi (2000), A new technique for rapid and non-destructive measurement of rock-surface moisture content; preliminary application to weathering studies of sandstone blocks, *Dev. Geotech. Eng.*, *84*, 47–54.
Mayaud, J. R., H. A. Viles, and M. A. Coombes (2014), Exploring the influence of biofilm on short-term expansion and contraction of supratidal rock: An example from the Mediterranean, *Earth Surf. Processes Landforms*, *39*(10), 1404–1412.
McAllister, D., P. Warke, and S. McCabe (2017), Stone temperature and moisture variability under temperate environmental conditions: Implications for sandstone weathering, *Geomorphology*, *280*, 137–152.
McAllister, D., P. Warke, S. McCabe, and M. Gomez-Heras (2016), Evaporative moisture loss from heterogeneous stone: Material-environment interactions during drying, *Geomorphology*, *273*, 308–322.
McAuliffe, J. R., L. A. Scuderi, and L. D. McFadden (2006), Tree-ring record of hillslope erosion and valley floor dynamics: Landscape responses to climate variation during the last 400 yr in the Colorado Plateau, northeastern Arizona, *Global Planet. Change*, *50*(3), 184–201.
McCabe, S., B. Smith, and P. Warke (2007), Preliminary observations on the impact of complex stress histories on sandstone response to salt weathering: Laboratory simulations of process combinations, *Environ. Geol.*, *52*(2), 251–258.
McFadden, L. D. (2013), Strongly dust-influenced soils and what they tell us about landscape dynamics in vegetated aridlands of the southwestern United States, *Geol. Soc. Am. Spec. Pap.*, *500*, 501–532.
McKay, C. P., J. L. Molaro, and M. M. Marinova (2009), High-frequency rock temperature data from hyper-arid desert environments in the Atacama and the Antarctic Dry Valleys and implications for rock weathering, *Geomorphology*, *110*(3), 182–187.
Meredith, P., and B. Atkinson (1983), Stress corrosion and acoustic emission during tensile crack propagation in Whin Sill dolerite and other basic rocks, *Geophys. J. Int.*, *75*(1), 1–21.
Meredith, P., and B. Atkinson (1985), Fracture toughness and subcritical crack growth during high-temperature tensile deformation of Westerly granite and black gabbro, *Phys. Earth Planet. In.*, *39*(1), 33–51.
Meredith, P. G. (1990), Fracture and failure of brittle polycrystals: An overview, in *Deformation Processes in Minerals, Ceramics and Rocks*, pp. 5–47, Springer, New York.
Meredith, P. G., K. S. Knight, S. A. Boon, and I. G. Wood (2001), The microscopic origin of thermal cracking in rocks: An investigation by simultaneous time-of-flight neutron diffraction and acoustic emission monitoring, *Geophys. Res. Lett.*, *28*(10), 2105–2108.
Michalske, T. A., and S. W. Freiman (1982), A molecular interpretation of stress corrosion in silica, *Nature*, *295*, 511–512.
Mol, L., and H. A. Viles (2012), The role of rock surface hardness and internal moisture in tafoni development in sandstone, *Earth Surf. Processes Landforms*, *37*(3), 301–314.
Molaro, J., and S. Byrne (2015), Grain-scale thermoelastic stresses and spatiotemporal temperature gradients on airless bodies, implications for rock breakdown, *J. Geophys. Res. Planets*, *120*, 255–277, doi:10.1002/2014JE004729.
Molaro, J. L., S. Byrne, and J.-L. Le (2017), Thermally induced stresses in boulders on airless body surfaces, and implications for rock breakdown, *Icarus*, doi:10.1016/j.icarus.2017.03.008.
Molnar, P. (2004), Interactions among topographically induced elastic stress, static fatigue, and valley incision, *J. Geophys. Res.*, *109*, F02010, doi:10.1029/2003JF000097.
Moores, J. E., J. D. Pelletier, and P. H. Smith (2008), Crack propagation by differential insolation on desert surface clasts, *Geomorphology*, *102*(3), 472–481.
Moses, C., D. Robinson, and J. Barlow (2014), Methods for measuring rock surface weathering and erosion: A critical review, *Earth Sci. Rev.*, *135*, 141–161.
Mushkin, A., A. Sagy, E. Trabelci, R. Amit, and N. Porat (2014), Measuring the time and scale-dependency of subaerial rock weathering rates over geologic time scales with ground-based lidar, *Geology*, *42*(12), 1063–1066.
Nara, Y., and K. Kaneko (2006), Sub-critical crack growth in anisotropic rock, *Int. J. Rock Mech. Min. Sci.*, *43*(3), 437–453.
Nara, Y., N. Hiroyoshi, T. Yoneda, and K. Kaneko (2010), Effects of relative humidity and temperature on subcritical crack growth in igneous rock, *Int. J. Rock Mech. Min. Sci.*, *47*(4), 640–646.
Nara, Y., H. Yamanaka, Y. Oe, and K. Kaneko (2013), Influence of temperature and water on subcritical crack growth parameters and long-term strength for igneous rocks, *Geophys. J. Int.*, *193*(1), 47–60.
Nara, Y., K. Kashiwaya, Y. Nishida, and T. Ii (2017), Influence of surrounding environment on subcritical crack growth in marble, *Tectonophysics*, *706-707*, 116–128.
Nara, Y., K. Morimoto, T. Yoneda, N. Hiroyoshi, and K. Kaneko (2011), Effects of humidity and temperature on subcritical crack growth in sandstone, *Int. J. Solids Struct.*, *48*(7), 1130–1140.
Nasseri, M., B. Mohanty, and P.-Y. Robin (2005), Characterization of microstructures and fracture toughness in five granitic rocks, *Int. J. Rock Mech. Min. Sci.*, *42*(3), 450–460.
Nicolas, B., H. Michael, B. Patrick, and M. Philip (2014), Brittle vs ductile creep in porous limestone, 10 th Euroconference on Rock Physics and Rock Mechanics, 68.
Nowacki, W. (2013), *Thermoelasticity*, Elsevier, Amsterdam, Netherlands.
Ollier, C. (1984), *Weathering*, Longman Group, Essex, U. K.
Olson, J. E. (2004), Predicting fracture swarms—The influence of subcritical crack growth and the crack-tip process zone on joint spacing in rock, *Geol. Soc. London, Spec. Publ.*, *231*(1), 73–88.
Ouchterlony, F. (1990), Fracture toughness testing of rock with core based specimens, *Eng. Fract. Mech.*, *35*(1), 351–366.

Owen, J. J., R. Amundson, W. E. Dietrich, K. Nishiizumi, B. Sutter, and G. Chong (2011), The sensitivity of hillslope bedrock erosion to precipitation, *Earth Surf. Processes Landforms*, *36*(1), 117–135.
Paris, P. C., M. P. Gomez, and W. E. Anderson (1961), A rational analytic theory of fatigue, *The trend in engineering*, *13*(1), 9–14.
Parkins, R. (2005), Stress corrosion cracking, in *Uhlig's Corrosion Handbook*, vol. 191, pp. 171–181, John Wiley, Hoboken, N. J.
Parks, G. A. (1984), Surface and interfacial free energies of quartz, *J. Geophys. Res.*, *89*(B6), 3997–4008.
Passchier, C. W., and R. Trouw (2005), Deformation mechanisms, *Microtectonics*, *25-66*.
Pelletier, J. D., and T. L. Swetnam (2017), Asymmetry of weathering-limited hillslopes: The importance of diurnal covariation in solar insolation and temperature, *Earth Surf. Processes Landforms*, doi:10.1002/esp.4136.
Perron, J. T. (2017), Climate and the pace of erosional landscape evolution, *Annu. Rev. Earth Planet. Sci.*, *45*(1).
Persico, L. P., L. D. McFadden, J. D. Frechette, and G. A. Meyer (2011), Rock type and dust influx control accretionary soil development on hillslopes in the Sandia Mountains, New Mexico, USA, *Quatern. Res.*, *76*(3), 411–416.
Portenga, E. W., and P. R. Bierman (2011), Understanding Earth's eroding surface with 10 Be, *GSA Today*, *21*(8), 4–10.
Potyondy, D. O. (2007), Simulating stress corrosion with a bonded-particle model for rock, *Int. J. Rock Mech. Min. Sci.*, *44*(5), 677–691.
Raja, V., and T. Shoji (2011), *Stress Corrosion Cracking: Theory and Practice*, Woodhead, Cambridge, U. K.
Ravina, I., and D. Zaslavsky (1974), The electrical double layer as a possible factor in desert weathering, *Z. Geomorphol.*, *21*, 13–18.
Reed, G., and A. B. Klugh (1924), Correlation between hydrogen ion concentration and biota of granite and limestone pools, *Ecology*, *5*(3), 272–275.
Robertson, E. C. (1988), Thermal properties of rocks Rep. 2331–1258, U.S. Geological Survey.
Rode, M., H. Schnepfleitner, and O. Sass (2016), Simulation of moisture content in alpine rockwalls during freeze–thaw events, *Earth Surf. Processes Landforms*, *41*(13), 1937–1950.
Roering, J. J., J. Marshall, A. M. Booth, M. Mort, and Q. Jin (2010), Evidence for biotic controls on topography and soil production, *Earth Planet. Sci. Lett.*, *298*(1), 183–190.
Røyne, A., J. Bisschop, and D. K. Dysthe (2011), Experimental investigation of surface energy and subcritical crack growth in calcite, *J. Geophys. Res.*, *116*, B04204, doi:10.1029/2010JB008033.
Rubin, A. M. (1993), Tensile fracture of rock at high confining pressure: Implications for dike propagation, *J. Geophys. Res.*, *98*(B9), 15,919–15,935.
Ryb, U., A. Matmon, Y. Erel, I. Haviv, A. Katz, A. Starinsky, A. Angert, and A. Team (2014), Controls on denudation rates in tectonically stable Mediterranean carbonate terrain, *Geol. Soc. Am. Bull.*, *126*(3–4), 553–568.
Sass, O. (2005), Rock moisture measurements: Techniques, results, and implications for weathering, *Earth Surf. Processes Landforms*, *30*(3), 359–374.
Schnepfleitner, H., O. Sass, S. Fruhmann, H. Viles, and A. Goudie (2015), A multi-method investigation of temperature, moisture and salt dynamics in tafoni (Tafraoute, Morocco), *Earth Surf. Processes Landforms*, *41*, 473–485.
Shobe, C. M., et al. (2017), Field evidence for the influence of weathering on rock erodibility and channel form in bedrock rivers, *Earth Surf. Processes Landforms*, doi:10.1002/esp.4163
Scholz, C., and R. Kranz (1974), Notes on dilatancy recovery, *J. Geophys. Res.*, *79*(14), 2132–2135.
Scholz, C., and T. Koczynski (1979), Dilatancy anisotropy and the response of rock to large cyclic loads, *J. Geophys. Res.*, *84*(B10), 5525–5534.
Shi, J. (2011), *Study of Thermal Stresses in Rock Due to Diurnal Solar Exposure*, 103 pp., Univ. of Wash., Seattle.
Siegesmund, S., K. Ullemeyer, T. Weiss, and E. Tschegg (2000), Physical weathering of marbles caused by anisotropic thermal expansion, *Int. J. Earth Sci.*, *89*(1), 170–182.
Siman-Tov, S., O. Katz, and A. Matmon (2017), Examining the effects of ground motion and rock strength on the size of boulders falling from an overhanging cliff, *Eng. Geol.*, *220*, 164–174.
Siren, T. (2012), Fracture toughness properties of rocks in Olkiluoto: Laboratory measurements 2008–2009, Rep. POSIVA-WR–12-25, Posiva Oy.
Skinner, B. J. (1966), Section 6: Thermal expansion, *Geol. Soc. Am. Mem.*, *97*, 75–96.
Small, E. E., R. S. Anderson, and G. S. Hancock (1999), Estimates of the rate of regolith production using 10Be and 26Al from an alpine hillslope, *Geomorphology*, *27*(1), 131–150.
Smith, B., S. Srinivasan, M. Gomez-Heras, P. Basheer, and H. Viles (2011), Near-surface temperature cycling of stone and its implications for scales of surface deterioration, *Geomorphology*, *130*(1), 76–82.
Sousa, L. M., L. M. S. del Río, L. Calleja, V. G. R. de Argandona, and A. R. Rey (2005), Influence of microfractures and porosity on the physico-mechanical properties and weathering of ornamental granites, *Eng. Geol.*, *77*(1), 153–168.
St. Clair, J. S., S. Moon, W. Holbrook, J. Perron, C. Riebe, S. Martel, B. Carr, C. Harman, and K. Singha (2015), Geophysical imaging reveals topographic stress control of bedrock weathering, *Science*, *350*(6260), 534–538.
Stephens, R., H. W. Lee, R. Bu, and G. K. Werner (1988), The behavior of short and long fatigue cracks at threshold and near-threshold levels, paper presented at Fracture Mechanics: Eighteenth Symposium, ASTM International.
Stock, G. M., S. J. Martel, B. D. Collins, and E. L. Harp (2012), Progressive failure of sheeted rock slopes: The 2009–2010 Rhombus Wall rock falls in Yosemite Valley, California, USA, *Earth Surf. Processes Landforms*, *37*(5), 546–561.
Stück, H., R. Plagge, and S. Siegesmund (2013), Numerical modeling of moisture transport in sandstone: The influence of pore space, fabric and clay content, *Environ. Earth Sci.*, *69*(4), 1161–1187.
Sumner, P., W. Nel, and D. Hedding (2004), Thermal attributes of rock weathering: Zonal or azonal? A comparison of rock temperatures in different environments, *Polar Geogr.*, *28*(2), 79–92.
Sumner, P., D. Hedding, and K. Meiklejohn (2007), Rock surface temperatures in southern Namibia and implications for thermally-driven physical weathering, *Z. Geomorphol.*, *51*(1), 133–147.
Swanson, P. L. (1984), Subcritical crack growth and other time-and environment-dependent behavior in crustal rocks, *J. Geophys. Res.*, *89*(B6), 4137–4152.
Tanigawa, Y., and Y. Takeuti (1983), Three-dimensional thermoelastic treatment in spherical region and its application to solid sphere due to rotating heat source, *ZAMM-Journal of Applied Mathematics and Mechanics/Zeitschrift für Angewandte Mathematik und Mechanik*, *63*(7), 317–324.
Tharp, T. M. (1987), Conditions for crack propagation by frost wedging, *Geol. Soc. Am. Bull.*, *99*(1), 94–102.
Tratebas, A. M., N. V. Cerveny, and R. I. Dorn (2004), The effects of fire on rock art: Microscopic evidence reveals the importance of weathering rinds, *Phys. Geogr.*, *25*(4), 313–333.
Turkington, A. V., and T. R. Paradise (2005), Sandstone weathering: A century of research and innovation, *Geomorphology*, *67*(1), 229–253.
Twidale, C. R., and J. R. V. Romaní (2005), *Landforms and Geology of Granite Terrains*, CRC Press, London, U. K.

Vasile, M., and A. Vespremeanu-Stroe (2016), Thermal weathering of granite spheroidal boulders in a dry-temperate climate, Northern Dobrogea, Romania, *Earth Surf. Processes Landforms*, *42*, 259–271, doi:10.1002/esp.3984.
Vázquez, M., S. Ramírez, D. Morata, M. Reich, J.-J. Braun, and S. Carretier (2016), Regolith production and chemical weathering of granitic rocks in central Chile, *Chem. Geol.*, *446*, 87–98.
Vázquez, P., V. Shushakova, and M. Gómez-Heras (2015), Influence of mineralogy on granite decay induced by temperature increase: Experimental observations and stress simulation, *Eng. Geol.*, *189*, 58–67.
Viles, H. A. (2005), Microclimate and weathering in the central Namib Desert, Namibia, *Geomorphology*, *67*(1), 189–209.
Viles, H. A. (2012), Microbial geomorphology: A neglected link between life and landscape, *Geomorphology*, *157*, 6–16.
Von Blanckenburg, F. (2005), The control mechanisms of erosion and weathering at basin scale from cosmogenic nuclides in river sediment, *Earth Planet. Sci. Lett.*, *237*(3), 462–479.
Walder, J., and B. Hallet (1985), A theoretical model of the fracture of rock during freezing, *Geol. Soc. Am. Bull.*, *96*(3), 336–346.
Wang, Z.-T., and Z.-S. An (2016), A simple theoretical approach to the thermal expansion mechanism of salt weathering, *Catena*, *147*, 695–698.
Warke, P., and B. Smith (1998), Effects of direct and indirect heating on the validity of rock weathering simulation studies and durability tests, *Geomorphology*, *22*(3), 347–357.
Warke, P. A., and B. J. Smith (2000), Salt distribution in clay-rich weathered sandstone, *Earth Surf. Processes Landforms*, *25*(12), 1333–1342.
Warren, K., M.-C. Eppes, S. Swami, J. Garbini, and J. Putkonen (2013), Automated field detection of rock fracturing, microclimate, and diurnal rock temperature and strain fields, *Geosci. Instrum. Method. Data Syst. Discuss.*, *3*(2), 371–406.
Waza, T., K. Kurita, and H. Mizutani (1980), The effect of water on the subcritical crack growth in silicate rocks, *Tectonophysics*, *67*(1–2), 25–34.
Weiss, T., S. Siegesmund, D. T. Kirchner, and J. Sippel (2004), Insolation weathering and hygric dilatation: Two competitive factors in stone degradation, *Environ. Geol.*, *46*(3–4), 402–413.
Wells, T., P. Binning, and G. Willgoose (2005), The role of moisture cycling in the weathering of a quartz chlorite schist in a tropical environment: Findings of a laboratory simulation, *Earth Surf. Processes Landforms*, *30*(4), 413–428.
Wells, T., G. Willgoose, and G. Hancock (2008), Modeling weathering pathways and processes of the fragmentation of salt weathered quartz-chlorite schist, *J. Geophys. Res.*, *113*, F01014, doi:10.1029/2006JF000714.
West, N., E. Kirby, P. Bierman, and B. A. Clarke (2014), Aspect-dependent variations in regolith creep revealed by meteoric 10Be, *Geology*, *42*(6), 507–510.
West, N., E. Kirby, P. Bierman, R. Slingerland, L. Ma, D. Rood, and S. Brantley (2013), Regolith production and transport at the Susquehanna Shale Hills Critical Zone Observatory, part 2: Insights from meteoric 10Be, *J. Geophys. Res. Earth*, *118*, 1877–1896, doi:10.1002/jgrf.20121.
Widhalm, C., E. Tschegg, and W. Eppensteiner (1996), Anisotropic thermal expansion causes deformation of marble claddings, *J. Perform. Constr. Facil*, *10*(1), 5–10.
Williams, R., and D. Robinson (1991), Frost weathering of rocks in the presence of salts-a review, *Permafr. Periglac. Process.*, *2*(4), 347–353.
Yao, M., G. Rong, C. Zhou, and J. Peng (2016), Effects of thermal damage and confining pressure on the mechanical properties of coarse marble, *Rock Mech. Rock Eng.*, *49*, 2043–2054.
Zhao, Y. (1998), Crack pattern evolution and a fractal damage constitutive model for rock, *Int. J. Rock Mech. Min. Sci.*, *35*(3), 349–366.
Zoback, M. D., and J. D. Byerlee (1975), The effect of cyclic differential stress on dilatancy in Westerly granite under uniaxial and triaxial conditions, *J. Geophys. Res.*, *80*(11), 1526–1530.